IMPLEMENTATION AND VERIFICATION OF RCWA MODEL

by

Genevieve Gish Allouche

A Thesis Submitted to the Faculty of the

COLLEGE OF OPTICAL SCIENCES

In Partial Fulfillment of the Requirements

For the Degree of

MASTER OF SCIENCE

In the Graduate College

THE UNIVERSITY OF ARIZONA
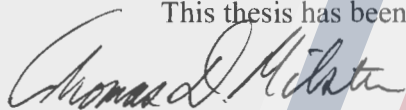
2018

STATEMENT BY THE AUTHOR

The thesis titled *Implementation and Verification of RCWA Model* prepared by Genevieve Gish Allouche has been submitted in partial fulfillment of requirements for a master's degree at the University of Arizona and is deposited in the University Library to be made available to borrowers under rules of the Library.

Brief quotations from this thesis are allowable without special permission, provided that an accurate acknowledgement of the source is made. Requests for permission for extended quotation from or reproduction of this manuscript in whole or in part may be granted by the head of the major department or the Dean of the Graduate College when in his or her judgment the proposed use of the material is in the interests of scholarship. In all other instances, however, permission must be obtained from the author.

SIGNED: *Genevieve Gish Allouche*
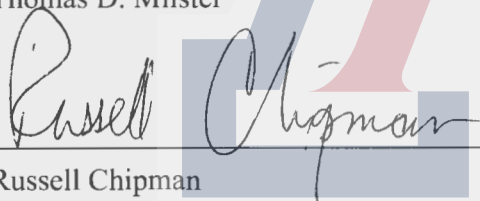
APPROVAL BY THESIS DIRECTOR

This thesis has been approved on the date shown below:

Thomas D. Milster	08/10/2018 Date
Russell Chipman	08/10/2018 Date
Chris Kocot	08/10/2018 Date

ACKNOWLEDGMENTS

TABLE OF CONTENTS

LIST OF FIGURES

LIST OF TABLES

ABSTRACT

An RCWA Matlab simulation was developed to guide future designs of phase plates for VCSELs. We will discuss the verification process to validate our current model. Moreover, we will compare and contrast these results from the ones obtained from other software models, Polaris-M and OptiScan. A comparison between theoretical and experimental results will further test the validity of the model. Our second goal is to demonstrate experimentally Rayleigh anomalies, predicted by Harvey and Pfisterer's non-paraxial scalar theory.

Chapter 1 – Introduction

According to Sommerfeld, diffraction is defined as "any deviation of light rays from rectilinear paths which cannot be interpreted as reflection or refraction." [1] Huygens stated that the field distribution at the aperture is composed of an infinite number of secondary sources, which is shown in the Huygens-Fresnel principle.

$$U(P_0) = \frac{1}{j\lambda} \iint U(P_1) \frac{exp(jkr_{01})}{r_{01}} cos\theta ds \qquad (1)$$

Where θ is the angle between $\vec{n}$ and $\vec{r}_{01}$. It expresses the observed field as a superposition of spherical waves originating from secondary sources within an aperture. An assumption associated with this principle is that the observation distance is many wavelengths away from the aperture, i.e. $r_{01} \square \lambda$. Another assumption is associated with scalar theory. It is accurate if the following two conditions are met: 1) the aperture must be large compared to the wavelength of the source and 2) the diffracting fields must not be observed too close to the aperture [2]. In general, Huygens-Fresnel principle accurately describes the diffraction pattern depending on a given aperture. However, similar to every model, it has its limitations. Since this thesis will examine the diffraction occurring at a grating, then the aperture may not follow the first condition of scalar theory. A solution to this dilemma is Rigorous Coupled Wave Analysis (RCWA).

RCWA is a powerful, semi-analytical method to numerically investigate the optical properties of sub-wavelength gratings. This numerically solves Maxwell's equations in the Fourier domain to illustrate the behavior of an incident electric field as it propagates through a system, defined as a discrete number of layers. The resulting transmitted and reflected electric

fields are observed by calculating the eigenvectors of each layer. The multilayer framework combines the eigenvectors of each layer to observe the system as a whole. In the end, the reflected and transmitted fields of the entire system can be examined, as well as their corresponding diffraction efficiencies.

However, Harvey and Pfisterer argue that scalar diffraction theory can be extended to the non-paraxial regime. They were able to verify this theory against a rigorous model as shown in Figure 1. The non-paraxial scalar diffraction theory also predicts the Rayleigh anomalies, which is "a rapid variation of the photometric efficiency of a grating over a […] short range of wavelengths." [3] There is a redistribution of light for each diffracted order as they become evanescent.
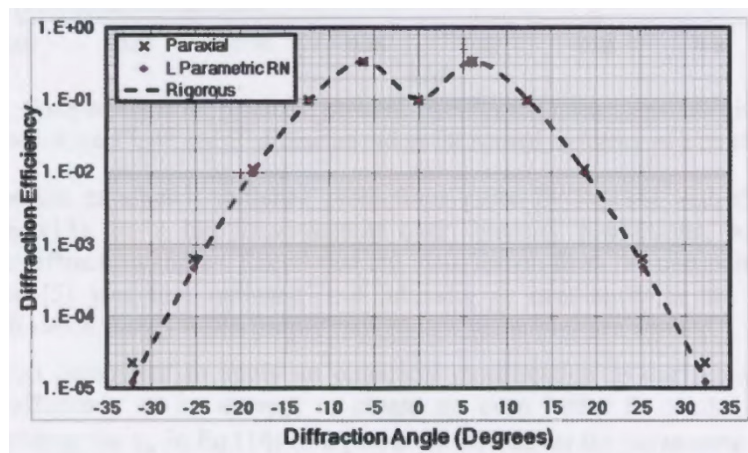
Figure 1 - Comparison of predicted diffraction efficiencies for normal incidence and near-paraxial diffracted angles [4]

This thesis discusses our development of a user-friendly RCWA model in Matlab to guide future grating designs. There is a discussion about the verification steps required to test the validity of the model. The theoretical results from this model are also compared against Polaris-M, OptiScan, and experimental data. In addition, this thesis will verify the non-paraxial diffraction model by observing the Rayleigh anomalies experimentally.

Chapter 2 – Background

Geometrical optics is the study of light propagating through a system in the limit of short wavelengths. However, this does not include diffraction, polarization, and quantum effects. The understanding of waves begins with Maxwell's equations, which describe material properties and the behavior of light in three-dimensional space. Materials are defined by their density of total charge, total current, atomic electric dipole moments (i.e., polarization), atomic magnetic dipole moments (i.e., magnetization), permittivity, and permeability. Permittivity, also known as a dielectric function, describes the amount of charge needed to generate one unit of electric flux in a medium. The microscopic Maxwell's equations, where the polarization and magnetization of a material are non-existent, will be the primary focus. Light waves are described in terms of their electric and magnetic fields. The polarization of light refers to the oscillation direction. *S* and *p* polarizations are the adopted conventions in optics, oriented perpendicular and parallel to the plane of incidence, respectively. From Maxwell's equations, the plane-wave solution is derived.

From the wave equation, Maxwell's equations can be reduced down to the Helmholtz equation, if there is a lack of current in the material. The Helmholtz equation, a second-order ordinary differential equation,

$$(\nabla^2 + k^2)E = 0 \qquad (2)$$

defines plane wave solutions. When there is a lack of free charge and electric potential, the electric field has the following solution:

$$E(\vec{r}, t) = E_0 e^{i(\vec{k} \cdot \vec{r} - \omega t)} \qquad (3)$$

where ω is the oscillation frequency, $\vec{k}$ is the propagation vector, and $\vec{E}_0$ is the amplitude and polarization vector of the electric field. A solution to the equation is a plane wave propagating in the **k**-direction. The Helmholtz equation also introduces a constraint on **k**:

$$k_x^2 + k_y^2 + k_z^2 = \omega^2 \mu \epsilon \qquad (4)$$

The exponential term in the plane wave solution describes a surface of constant phase, where $\vec{k} \cdot \vec{r} = constant$. The wave fronts are separated by the wavelength.

Gratings have a periodic structure and diffract light into multiple orders. There are different types of gratings with varying thicknesses. For example, reflection gratings only reflect light whereas others both reflect and transmit light. This thesis will specifically examine thin gratings with a classical plane-wave illumination, as shown below in Figure 2.
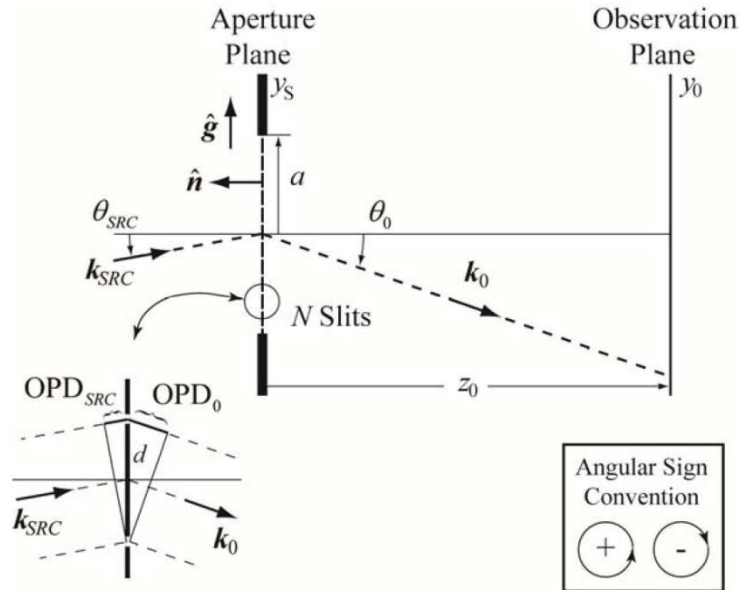
Figure 2 - Grating with plane-wave illumination [5]

Between each slit, the total optical path difference (OPD) to the observation point is the sum of the OPD_{source} and OPD_0. Constructive interference occurs when the following equation holds true:

$$n_{src}sin(\theta_{src}) - n_0 sin(\theta_m) = \frac{m\lambda}{d}$$

(5)

where n_{src} and n_0 are the refractive indices on the illumination and observation sides, respectively. For notation purposes, θ_m is synonymous to θ_0. This equation is commonly referred as the grating equation, which only predicts the directions of the modes, not the emitted power. The bright spots are referred as the diffraction orders, which correspond to the number of wavelengths of OPD. Figure 3 illustrates the followed convention.
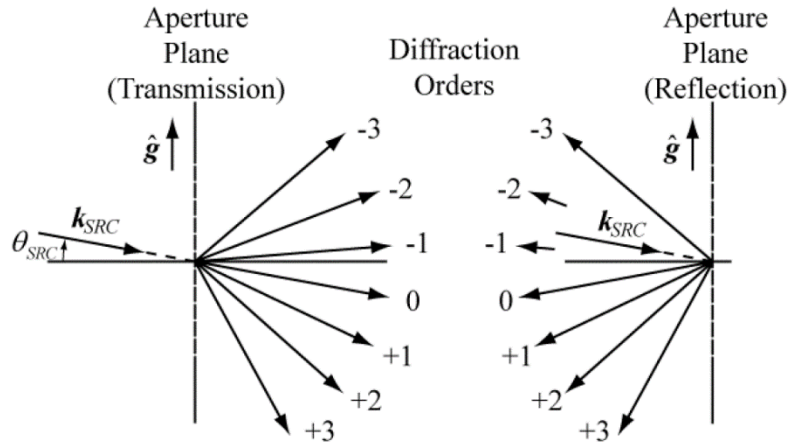
Figure 3 - Diffraction orders of grating with plane-wave illumination [5]

Rigorous coupled wave analysis developed in multiple stages. Each introduced new numerical methods and expanded the possible applications. From the early 1960s to the early 1970s, a basic rigorous coupled wave analysis was developed utilizing the integral and differential methods [6]. At this time, electromagnetic theory of gratings began. Coupled wave theory and modal theory were utilized in conjunction. The coupled wave theory assumed a

monochromatic source incident on the grating near the Bragg angle and polarized perpendicular to the plane of incidence (i.e., *s* polarized light). The propagation constant is related to the dielectric constant and conductivity of the medium, while the total electric field is defined as the superposition of the reference and signal wave. Kogelnik used coupled wave theory to predict the maximum efficiencies of certain types of holograms, as well as wavelength and angular dependence at higher diffraction efficiencies [7]. The modal theory is specifically used for periodic structures. The amplitudes of the EM waves are determined by looking at boundary conditions for each component [8]. These two methods together solved the scalar wave equation to determine the reference and signal EM waves. These prior methods depended on approximations. Therefore, they did not obtain an exact solution. By the time we reached the early 1990s to the present, the research improved the existing methods in numerical stability and convergence speed.

Moharam and Gaylord developed a rigorous coupled-wave analysis in the early 1980s, an improvement on the previous methods, where they obtained an exact solution to Maxwell's equations. They examined the diffraction of a plane wave incident on a planar grating bounded by two different media [9] and dielectric surface-relief gratings. The rigorous method solved the wave equation in a simple matrix format, which is a straightforward eigenvalue problem. These differential equations calculated the electric and magnetic fields at a specific point using only information from the local vicinity, thus requiring boundary conditions. They examined the diffraction efficiencies of the transmitted waves as they increased the thickness of the layer from sinusoidal phase (Figure 4), square-wave (Figure 5), triangular, and sawtooth/blazed gratings [10]. RCWA allowed them to observe the variation in the transmitted diffraction efficiencies for each diffracted order.

As the complexity of a grating increased, Rumpf incorporated scattering matrices to establish a relationship between each layer [11], which are uniform in the longitudinal direction (i.e., z-direction). Bands of free space with zero thickness are defined between the layers. So, the scatter matrix of each type of layer is calculated regardless of the neighboring materials. For longitudinally periodic devices, the scattering matrices can be reused. Only two parameters are calculated rather than four parameters simplifying the calculation further due to the symmetry of the device. Once the scattering matrices are combined, the grating is examined as an entire system.

The rigorous method can be used to examine the anomalous effects, i.e. Rayleigh or Woods anomalies, which do not behave according to ordinary grating theory. In 1902, Woods discovered a rapid change in the intensity of certain diffracted orders in a narrow frequency band caused by reflection diffraction gratings. In addition to the reflected wave, specified by the 0th diffraction order, there are higher multiple orders. As he altered the source wavelength, he
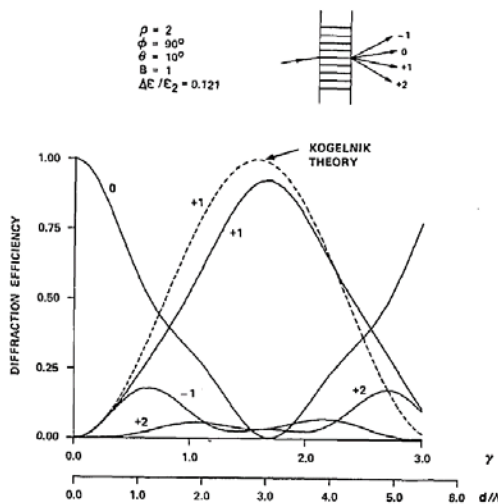
Figure 4 - Diffraction efficiencies of transmitted waves from a sinusoidal phase grating [10]
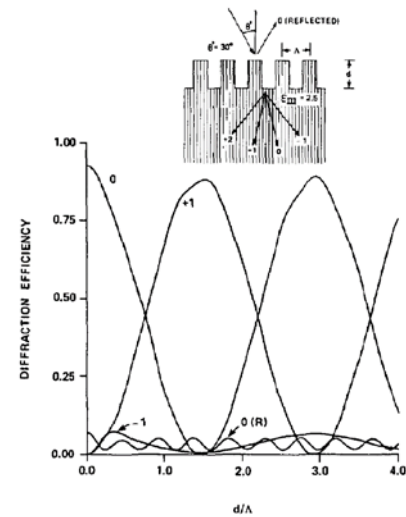
Figure 5 - Diffraction efficiencies as a function of groove depth for an ideal square-wave grating [10]

tracked one of the orders, such as n = 1, while the n = 0 wave remained in the same position. The amplitude versus wavelength of a specific order was shown to be a significant change in

intensity. There are in fact two anomalous effects occurring: 1) a rapid variation in the amplitudes of the diffracted orders due to the presence or disappearance of a particular order, and 2) a resonance type of behavior in these amplitudes [12]. The listed anomalies can either occur independently or in conjunction depending on the periodic structure.

Harvey predicted the Woods anomalies with his theory of scalar non-paraxial diffraction. Scalar diffraction theory, including Fresnel and Fraunhofer diffraction, are simple approximations utilizing Fourier transforms. However, they assume small diffracted and incident angles. Harvey demonstrated the linear, shift-invariant behavior of the diffracted radiance in terms of propagation vectors expressed as direction cosines [13]. A normalization factor followed the diffraction efficiency measurements from Wood's anomalies. It was also consistent with the conservation of energy.
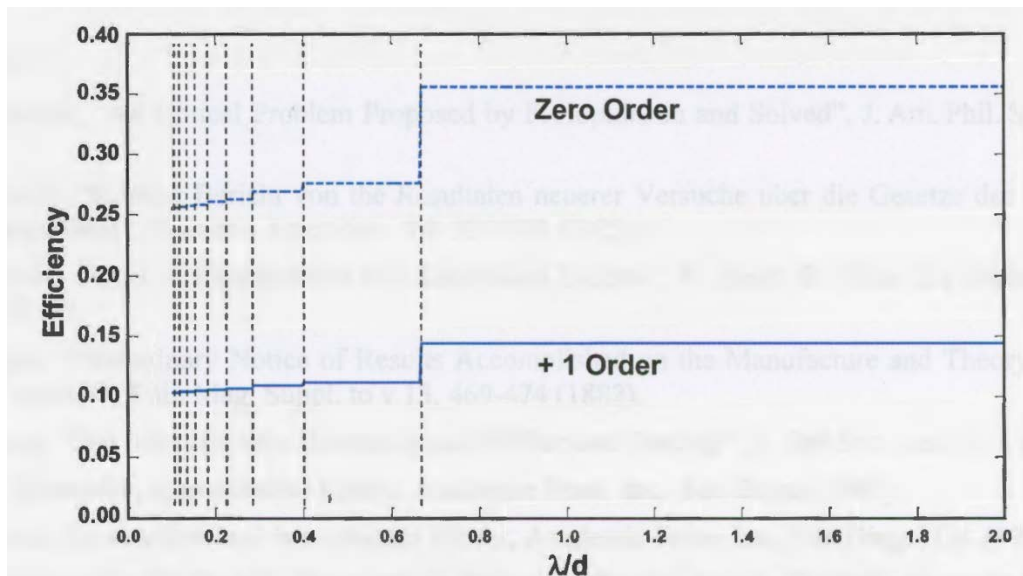
Figure 6 - Rayleigh anomalies from a square wave grating satisfying the +1 order Littrow condition [14]

RCWA can be applied to verify Harvey's theory of scalar non-paraxial diffraction. In 1999, Harvey developed this theory by using a linear systems approach. By applying the RCWA

method for a diffraction grating with an incident wave at a large angle, then the amount of error between the rigorous and scalar non-paraxial results can be determined.

Due to its simplicity and accuracy, RCWA was also used to simulate other types of structures, such as waveguides [15], liquid crystals [16], and Si high-contrast grating (HCG) reflector on VCSELs [17]. In these cases, the rigorous method was used for subwavelength gratings. When looking specifically at the last example, the overall dimensions ranged a large spectrum. The HCG has a period close to the incident wavelength and a large refractive index contrast between the grating bars and surrounding material. In order to simulate HCG-based cavities, the entire domain was on the order of tens of μm while the smallest characteristic dimensions were on the order of hundreds of nm. RCWA was a quick and simple method of solving Maxwell's equations for HCGs.

Due to the rapid and simple nature of RCWA, its rise in popularity of simulating optical systems is shown by the collection of commercial and open source software on the market. Airy Optics based in Arizona developed the RCWA simulation within Polaris-M [18], which is built from the Mathematica environment. DiffractMOD from Synopsis [19] is another commercial software on the market, fully integrated into the RSoft CAD environment. In addition to commercial software, open source programs created through universities are open to the public, such as S4 – Stanford Stratified Structure Solver from Stanford University [20]. The increase in available RCWA software illustrates the gain in popularity of the method for research.

Chapter 3 – Theory of RCWA model

3.1. Solving the matrix-form of the wave equation

Rigorous coupled wave analysis is an exact solution to Maxwell's equations for a plane wave incident on a periodic structure. It analyzes the behavior of an electric field through a system of multiple, periodic layers by solving Maxwell's equations in the Fourier domain, as shown in Figure 7. Each layer is homogeneous in the z-direction, defined with a thickness, corresponding spatial periods in the x and y-directions as well as dielectric constant including absorption. The general EM field is defined by the propagation vector $\vec{k}_{inc}$ and the amplitudes in the *s* and *p* directions (i.e., perpendicular and parallel to the plane of incidence, respectively). Once the user sets up the layers and incident wave, RCWA determines the transmitted and reflected fields by the method described below.

As a quick overview, listed are the main steps of RCWA:

1. Convert two equations from Maxwell's equations, the curl of the electric and magnetic fields, to the Fourier domain
2. Rewrite these equations in block matrix format
3. Determine the matrices **P** and **Q** with the diagonal matrices $\mathbf{K_x}$ and $\mathbf{K_y}$
4. Solve eigenvalue problem to determine matrices **W** and **V**, which are related to properties of a specific layer
5. Repeat steps 1-4 for each layer
6. Combine information from each layer to calculate the scattering matrix of the entire system
7. Determine the reflected and transmitted fields
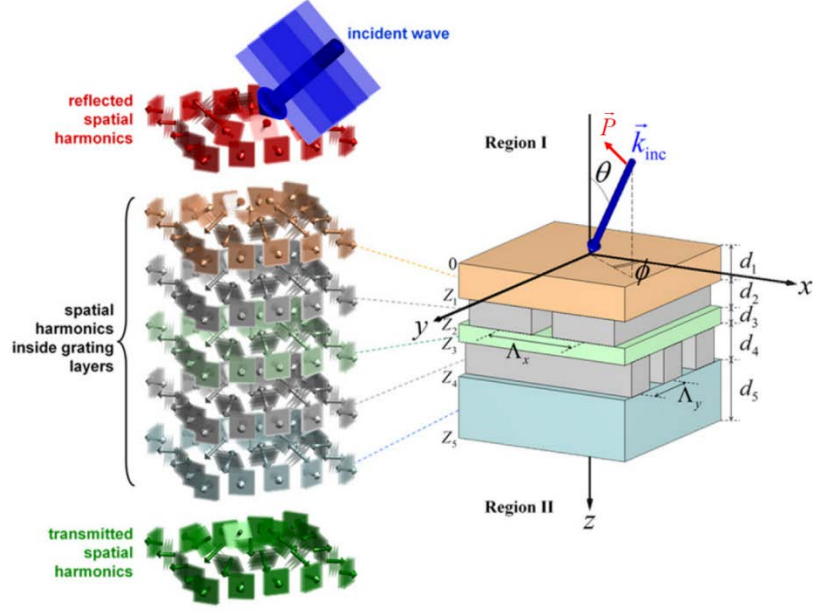
Figure 7 - Geometry of general RCWA setup [21]

The rigorous method begins by looking at the microscopic version of Maxwell's equations, where **P** and **M** are equal to zero. **P** and **M** correspond to the polarization and magnetization of the material. Equations (6) and (7), i.e. Ampere's and Faraday's law, relate the electric and magnetic fields with respect to one another.

$$\vec{\nabla} \cdot \vec{E} = \frac{\rho_{free}}{\epsilon} \tag{6}$$

$$\vec{\nabla} \times \vec{H} = \overrightarrow{J_{free}} + \epsilon \frac{\partial \vec{E}}{\partial t} \tag{7}$$

$$\vec{\nabla} \times \vec{E} = -\mu \frac{\partial \vec{H}}{\partial t} \tag{8}$$

$$\vec{\nabla} \cdot \vec{H} = 0 \tag{9}$$

After manipulating the partial derivative with respect to time and normalizing **H** to $-i\sqrt{\frac{\mu_0}{\epsilon_0}}\overrightarrow{H}$, then Equations (6) and (7) simplify to the following:

$$\vec{\nabla} \times \hat{H} = k_0 \epsilon_r \vec{E} \tag{10}$$

$$\vec{\nabla} \times \vec{E} = k_0 \mu_r \hat{H} \tag{11}$$

where $k_0 = \omega\sqrt{\grave{q}_0 \mu_0}$. Equations (9) and (10) are converted to the Fourier domain. **S** and **U** are the

2D Fourier transform coefficients of **E** and **H**, as shown below:

$$\vec{E}(x, y, z) = \sum_{m=-\infty}^{\infty} \sum_{n=-\infty}^{\infty} \vec{S}(m, n, z) e^{-j(k_x(m)x + k_y(n)y)} \tag{12}$$

$$\hat{H}(x, y, z) = \sum_{m=-\infty}^{\infty} \sum_{n=\infty}^{\infty} \vec{U}(m, n, z) e^{-j(k_x(m)x + k_y(n)y)} \tag{13}$$

The dielectric function and permeability are also converted to their corresponding Fourier series

expansions, defined by:

$$\epsilon_r(x, y) = \sum_{m=-\infty}^{\infty} \sum_{n=-\infty}^{\infty} a_{m,n} e^{j\left(\frac{2\pi mx}{\Lambda_x} + \frac{2\pi ny}{\Lambda_y}\right)} \tag{14}$$

$$\mu_r(x, y) = \sum_{m=-\infty}^{\infty} \sum_{n=-\infty}^{\infty} b_{m,n} e^{j\left(\frac{2\pi mx}{\Lambda_x} + \frac{2\pi ny}{\Lambda_y}\right)} \tag{15}$$

where $k_x(m) = k_{x,inc} - 2\pi m / \Lambda_x$ and $k_y(n) = k_{y,inc} - 2\pi n / \Lambda_y$. Λ_x and Λ_y refer to the periods in

the x and y directions as shown in Figure 7. Note, these equations are only valid for square or

rectangular symmetries. These Fourier expansions are inserted into the modified Maxwell's

equations. The z-components of **S** and **U** are eliminated, since the layers are homogeneous in the

z-direction. The expressions are rewritten in block matrix format:

$$\frac{\partial}{\partial \hat{z}} \begin{pmatrix} u_x \\ u_y \end{pmatrix} = Q \begin{pmatrix} s_x \\ s_y \end{pmatrix} \tag{16}$$

$$\frac{\partial}{\partial \hat{z}}\begin{pmatrix} s_x \\ s_y \end{pmatrix} = P\begin{pmatrix} u_x \\ u_y \end{pmatrix}$$ (17)

where $Q = \begin{pmatrix} \widehat{K_x}\mu_r^{-1}\widehat{K_y} & \epsilon_r - \widehat{K_x}\mu_r^{-1}\widehat{K_x} \\ \widehat{K_y}\mu_r^{-1}\widehat{K_y} - \epsilon_r & -\widehat{K_y}\mu_r^{-1}\widehat{K_x} \end{pmatrix}$ and $P = \begin{pmatrix} \widehat{K_x}\epsilon_r^{-1}\widehat{K_y} & \mu_r - \widehat{K_x}\epsilon_r^{-1}\widehat{K_x} \\ \widehat{K_y}\epsilon_r^{-1}\widehat{K_y} - \mu_r & -\widehat{K_y}\epsilon_r^{-1}\widehat{K_x} \end{pmatrix}$. $\hat{K}_x$

and $\hat{K}_y$ are diagonal matrices with elements $k_x(m)$ and $k_y(n)$. **P** and **Q** matrices can be

simplified further for the homogeneous case in the z-direction:

$$Q = \mu_r^{-1}\begin{pmatrix} \widehat{K_x}\widehat{K_y} & \epsilon_r\mu_r - \widehat{K_x}^2 \\ \widehat{K_y}^2 - \epsilon_r\mu_r I & -\widehat{K_y}\widehat{K_x} \end{pmatrix} = \frac{\epsilon_r}{\mu_r}P$$ (18)

$$P = \epsilon_r^{-1}\begin{pmatrix} \widehat{K_x}\widehat{K_y} & \mu_r\epsilon_r I - \widehat{K_x}^2 \\ \widehat{K_y}^2 - \mu_r\epsilon_r I & -\widehat{K_y}\widehat{K_x} \end{pmatrix}$$ (19)

By combining the **P** and **Q** matrices, the wave equation is written in terms of the **S** and **U**

components.

$$\frac{\partial^2}{\partial \hat{z}^2}S - \Omega^2 S = 0$$ (20)

where $\Omega^2 = PQ$. The general solutions of the wave equation solving for **S** and **U** are:

$$S = We^{-\lambda \hat{z}}c^+ + We^{\lambda \hat{z}}c^-$$ (21)

$$U = -Ve^{-\lambda \hat{z}}c^+ + Ve^{\lambda \hat{z}}c^-$$ (22)

where $c^+ = W^{-1}s^+(0)$, $c^- = W^{-1}s^-(0)$, and $V = QW\lambda^{-1}$. $s^+(0)$ and $s^-(0)$ are the initial values for

this differential equation. The superscripts $\pm$ indicates whether they pertain to the forward (+) or

backwards propagating waves (-). Let us combine these equations as shown below:

$$\psi(\hat{z}) = \begin{pmatrix} s_x(\hat{z}) \\ s_y(\hat{z}) \\ u_x(\hat{z}) \\ u_y(\hat{z}) \end{pmatrix} = \begin{pmatrix} W & W \\ -V & V \end{pmatrix} \begin{pmatrix} e^{-\lambda\hat{z}} & 0 \\ 0 & e^{\lambda\hat{z}} \end{pmatrix} \begin{pmatrix} c^+ \\ c^- \end{pmatrix} = \mathbf{W}\lambda C \tag{23}$$

Where the function ψ represents the overall solution which is the sum of all the modes at plane $\hat{z}$. $\mathbf{W}$ represents the square matrix whose column vectors describe the modes that can exist in the material, i.e. pictures of the modes which quantify the relative amplitudes $\mathbf{E_x}$, $\mathbf{E_y}$, $\mathbf{H_x}$, and $\mathbf{H_y}$. $e^{\lambda\hat{z}}$ is the diagonal matrix describing how the modes propagate, which includes accumulation of phase and decaying/growing amplitudes. $\mathbf{C}$ is the column vector containing the amplitude coefficient of each of the modes, i.e. quantifies the amount of energy in each mode. In the case of homogeneous layers, we can look at the eigenvectors ($\mathbf{W}$) and eigenvalues (λ^2) of Ω^2:

$$W = \begin{pmatrix} I & 0 \\ 0 & I \end{pmatrix} \tag{24}$$

$$\lambda = \begin{pmatrix} j\hat{K}_x & 0 \\ 0 & j\hat{K}_z \end{pmatrix} \tag{25}$$

The z-component of $\mathbf{K}$ is obtained from the dispersion relation: $\widehat{K_z} = \left(\sqrt{\mu_r \epsilon_r I - \widehat{K_x}^2 - \widehat{K_y}^2} \right)^*$.

The process of solving the wave equation is done for each layer individually. By combining the information from each layer, the behavior of an EM wave across the entire device is obtained.

3.2. Multilayer framework of scattering matrices
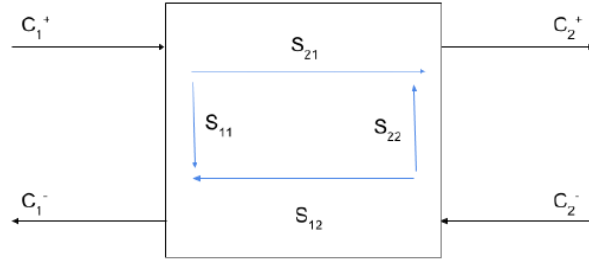
Figure 8 - Graphical representation of scatter matrix elements [11]

This semi-analytical method represents the system as a stack of layers. As shown in the previous section, each layer is defined by its corresponding eigenvectors and eigen-modes. A scattering matrix allows a complex structure to be represented as a "black box." The following expression relates the waves coming into the system to the ones departing the system:

$$\begin{pmatrix} c\,'^{-}_{1} \\ c\,'^{+}_{2} \end{pmatrix} = \begin{pmatrix} S_{11} & S_{12} \\ S_{21} & S_{22} \end{pmatrix} \begin{pmatrix} c\,'^{+}_{1} \\ c\,'^{-}_{2} \end{pmatrix} \tag{26}$$

where S_{11} and S_{21} represent the reflection and transmission, respectively. The boundary conditions require that all the layers have the same $\mathbf{K_x}$ and $\mathbf{K_y}$ matrices.

Once the scattering matrix for each layer is determined, a scattering matrix for the device as a whole is found. Let us assume free space with zero thickness is surrounding each layer, which allows for more flexibility in the calculation. Then, the elements of the scattering matrix are:

$$S_{11}^{(i)} = (A_i - X_i B_i A_i^{-1} X_i B_i)^{-1} (X_i B_i A_i^{-1} X_i A_i - B_i) \tag{27}$$

$$S_{12}^{(i)} = (A_i - X_i B_i A_i^{-1} X_i B_i)^{-1} X_i (A_i - B_i A_i^{-1} B_i) \tag{28}$$

$$S_{21}^{(i)} = S_{12}^{(i)} \tag{29}$$

$$S_{22}^{(i)} = S_{11}^{(i)} \tag{30}$$

where $A_{ij} = W_i^{-1}W_j + V_i^{-1}V_j$, $B_{ij} = W_i^{-1}W_j - V_i^{-1}V_j$, and $X_i = e^{-\lambda_i k_0 L_i}$. i represents the layer number

and j refers to the external medium on either side of the layer. For free space, j is equal to zero.

Since the layers are symmetric, the scattering matrix elements are redundant. Therefore,

Equations (28) and (29) hold true. This simplification allows us to diminish the number of

calculations and utilize less memory.

The scattering matrix of the device including its surroundings needs to be determined.

First, the scattering matrices of each layer are combined by applying the Redheffer star product.

For $S^{(AB)} = S^{(A)} \otimes S^{(B)}$, the resulting elements are:

$$S_{11}^{(AB)} = S_{11}^{(A)} + S_{12}^{(A)}[I - S_{11}^{(B)}S_{22}^{(A)}]^{-1}S_{11}^{(B)}S_{21}^{(A)} \tag{31}$$

$$S_{12}^{(AB)} = S_{12}^{(A)}[I - S_{11}^{(B)}S_{22}^{(A)}]^{-1}S_{12}^{(B)} \tag{32}$$

$$S_{21}^{(AB)} = S_{21}^{(B)}[I - S_{22}^{(A)}S_{11}^{B}]^{-1}S_{21}^{(A)} \tag{33}$$

$$S_{22}^{(AB)} = S_{22}^{(B)} + S_{21}^{(B)}[I - S_{22}^{(A)}S_{11}^{(B)}]^{-1}S_{22}^{(A)}S_{12}^{(B)} \tag{34}$$

Thus, a general scattering matrix for the entire system is defined.
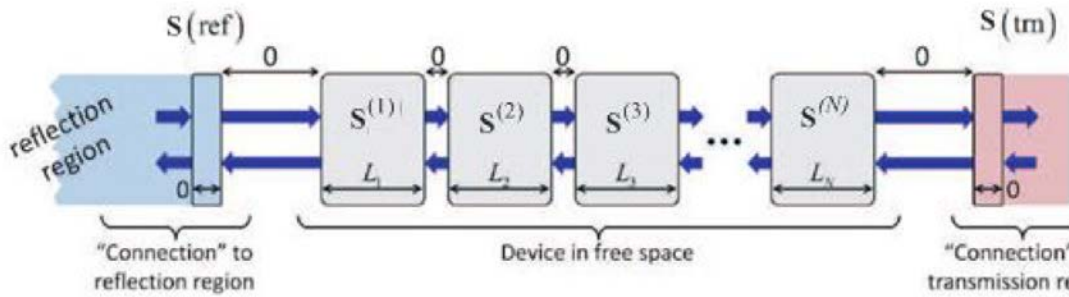
Figure 9 - Graphical representation of S matrices in a system [11]

Then, the connections to the reflection and transmission regions are incorporated to complete the

system by applying the Redheffer star product a second time: $S^{(global)} = S^{(r)} \otimes S^{(device)} \otimes S^{(t)}$. The

reflection side scattering matrix elements are:

$$S_{11}^{(r)} = -A_r^{-1} B_r \tag{35}$$

$$S_{12}^{(r)} = 2A_r^{-1} \tag{36}$$

$$S_{21}^{(r)} = 0.5(A_r - B_r A_r^{-1} B_r) \tag{37}$$

$$S_{22}^{(r)} = B_r A_r^{-1} \tag{38}$$

where $A_r = W_0^{-1} W_r + V_0^{-1} V_r$ and $B_r = W_0^{-1} W_r - V_0^{-1} V_r$. The transmission side scattering matrix

elements are defined as:

$$S_{11}^{(t)} = B_t A_t^{-1} \tag{39}$$

$$S_{12}^{(t)} = 0.5(A_t - B_t A_t^{-1} B_t) \tag{40}$$

$$S_{21}^{(t)} = 2A_t^{-1} \tag{41}$$

$$S_{22}^{(t)} = -A_t^{-1} B_t \tag{42}$$

where $A_t = W_0^{-1} W_t + V_0^{-1} V_t$ and $B_t = W_0^{-1} W_t - V_0^{-1} V_t$. Now, the scattering matrix of the entire

system is obtained.

The scattering matrix of the system provides information about the behavior of an EM

wave as it propagates through the device. These matrix elements determine the reflected and

transmitted diffraction efficiencies, as well as the reflectance and transmittance of the device.

3.3. Determining reflected and transmitted diffraction efficiencies

Once the scattering matrix is calculated for the entire system, the corresponding

reflected and transmitted diffraction efficiencies can be calculated. The transverse components

are determined by looking at the reflection and transmission elements derived from the scatter matrix:

$$r_T = s_T^r = W_r S_{11} c_{inc} \tag{43}$$

$$t_T = s_T^t = W_t S_{21} c_{inc} \tag{44}$$

Then, the corresponding longitudinal components can be found:

$$r_Z = -\hat{K}_{Z,r}^{-1}(\hat{K}_x r_x + \hat{K}_y r_y) \tag{45}$$

$$t_Z = -\hat{K}_{Z,t}^{-1}(\hat{K}_x t_x + \hat{K}_y t_y) \tag{46}$$

where $\hat{K}_{Z,r/t} = -(\sqrt{\mu_r \grave{o}_r I - \hat{K}_x^2} - \hat{K}_y)^*$ from the dispersion relation. The diffraction efficiencies are:

$$R = Re[\frac{-\hat{K}_{Z,r}}{k_{z,inc}}] \cdot |\vec{r}|^2 \tag{47}$$

$$T = Re[\frac{\mu_{r,inc}}{\mu_{r,t}} \frac{\hat{K}_{Z,t}}{k_{z,inc}}] \cdot |\vec{t}|^2 \tag{48}$$

The final results of RCWA are the reflected and transmitted electric fields, and the reflectance and transmittance of the system.**Chapter 4 - Implementation of RCWA in Matlab**

Inputs:
- Es and Ep
- Cells with all materials (names, permittivity)
- Struct with the order of the materials and their thicknesses

- Creates a struct with all the information needed
- Calculates W and V for each layer and saves in memory

- Finds projected E-field onto the first surface
- Converts E-field from space domain to Fourier domain

- Finds S matrix for entire device

Outputs:
- Determines reflected and transmitted fields in Fourier space
- Calculates reflectance and transmittance

Figure 10: Overall structure of RCWA model divided into four functions named: 1) layerInfo, 2) initializingStack, 3) stack_Scombine, and 4) rtCalc.

The program is designed to simulate the RCWA algorithm and can be used as a "black box." The user provides the incident electric fields in the *s* and *p* directions, materials with their corresponding dielectric functions, the order of the layers and their thicknesses. Cell arrays organize the different materials and their corresponding permittivity function. Structure arrays allow the user to specify the order of the layers. The number of materials from the cell is not required to correspond to the same size as the struct. The user can for example create a device alternating between two types of layers. However, all of the different layers need to appear in the structure array.

Once they provide the necessary information, the model runs through four separate functions: 1) *layerInfo()*, 2) *initializingStack()*, 3) *stack_Scombine()*, and 4) *rtCalc()*. The first step stores the layer information in the memory. The second function projects the three-dimensional electric field on the surface of the device and converts it to the Fourier domain. Then, the model calculates the scattering matrix for the entire system, which leads us to

determining the reflectance and transmittance. The reflected and transmitted electric fields are also obtained.
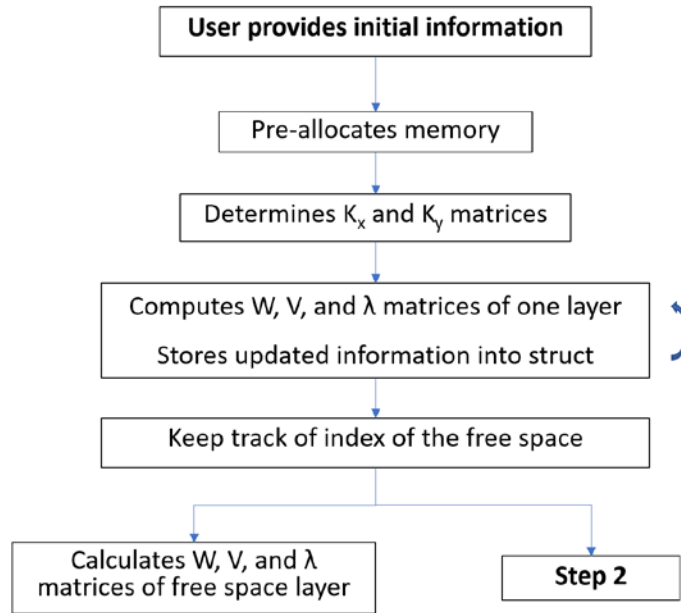
Figure 11 - Step 1: Specifying the properties of the layers

The first step specifies the properties of each layer and saves it in the memory. First, we pre-allocate memory to optimize the computation speed. Then, we determine the $\hat{K}_x$ and $\hat{K}_y$ matrices, which will remain the same for the entire device due to boundary conditions. For each layer, the program will calculate and store the **W**, **V**, and λ matrices, characterizing the existing modes in the material. These are equivalently properties of each layer. In the meantime, it keeps track of the location of the free space in the struct. If the free space is not listed, then the program will automatically add the information into the structure array.

The second step sets up the electric field to run the RCWA algorithm. First, the program checks if all the layers listed are included in the struct. If not, then an error prints in the command line. It will also keep track of the order of the layers in the structure array. Once all of

the possible positions and the number of Fourier coefficients are defined, then the program

projects the 3D electric field onto the first surface and converts it to the Fourier space.
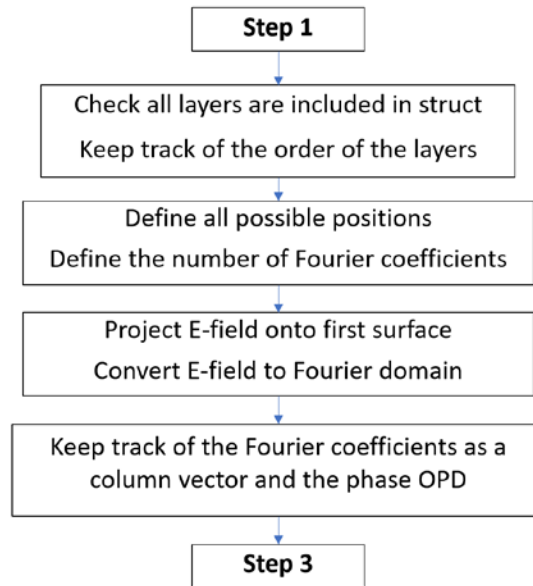
Figure 12 - Step 2: Setting up in the E-field
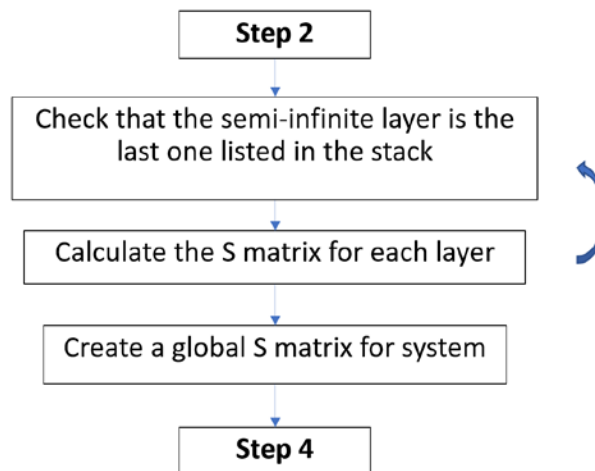
Figure 13 - Step 3: Creating a global scattering matrix

The third step involves determining the scattering matrices for the entire system. First,

the program will calculate the **S** matrix for each layer. Then, it will combine them all using the

Redheffer product.
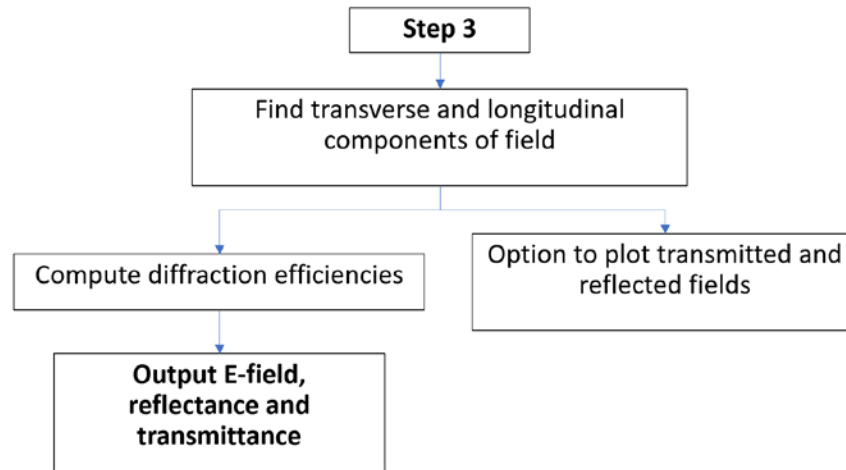
Figure 14 - Step 4: Calculating the reflectance, transmittance, reflected and transmitted fields

The fourth step involves finding the reflected and transmitted diffraction efficiencies. There is also an added option to plot the resulting transmitted and reflected fields, converted back to real space.

Chapter 5 – Verification steps

5.1. Checking glass/air interfaces

Let us start at the simplest case and slowly increase the level of complexity, one parameter at a time. The trivial case examines the electric field propagating at normal incidence in a vacuum, where the wave remains unchanged. Once homogeneous layers are added, then we can compare the RCWA results against the reflectance and transmittance obtained from the Fresnel equations. The reflectance of the *s* and *p* polarizations for homogeneous materials are:

$$R_s = \left| \frac{n_1 cos\theta_i - n_2 cos\theta_t}{n_1 cos\theta_i + n_2 cos\theta_t} \right|^2 \tag{49}$$

$$R_p = \left| \frac{n_1 cos\theta_t - n_2 cos\theta_i}{n_1 cos\theta_t + n_2 cos\theta_i} \right|^2 \tag{50}$$

where the transmission angle is determined by Snell's law:

$$n_1 sin\theta_i = n_2 sin\theta_t \tag{51}$$

n_1 and n_2 correspond to the incident and transmitted refractive indices. θ_i and θ_t are the incident and transmitted angles, respectively. The transmittance is calculated by subtracting the reflectance form unity, i.e. $T_s = 1 - R_s$ and $T_p = 1 - R_p$.

The RCWA model results align with the ones obtained from the Fresnel coefficients with the exception of one case. Tables 1 and 2 compare the reflectance and transmittance for plane waves propagating through an air/glass interface. As ϕ and θ vary, the RCWA results remain consistent with the Fresnel coefficients. The angle ϕ does not change the outcome of the reflectance and transmittance since the layers are homogeneous in the *xy*-plane. The reflectance and transmittance are examined, while varying the polarization of the incident electric fields. For

an incident *p*-polarized field, the RCWA results do not match the Fresnel coefficients as ϕ changes. Since the layers are homogeneous, the angle ϕ should not vary the outcome of the reflectance and transmittance. As shown in Figure 15, Brewster's angle due to the air/glass interface is clearly observed.

Table 1 - Checking RCWA results against Fresnel coefficients – Setting incident p-polarized E-field

ϕ (degrees)	θ (degrees)	RCWA result	Fresnel coefficients
0	0	R = 0.04, T = 0.96	R = 0.04, T = 0.96
20	0	R = 0.04, T = 0.96	R = 0.04, T = 0.96
0	20	R = 0.0335, T = 0.9665	Rp = 0.0335, Tp = 0.9665
0	45	Rp = 0.0085, Tp = 0.9915	Rp = 0.0085, Tp = 0.9915
15	45	Rp = 0.0179, Tp = 0.8571	Rp = 0.0085, Tp = 0.9915

Table 2 - Verifying RCWA results against Fresnel coefficients - Setting incident s-polarized plane wave

ϕ (degrees)	θ (degrees)	RCWA result	Fresnel coefficients
0	0	R = 0.04, T = 0.96	R = 0.04, T = 0.96
20	0	R = 0.04, T = 0.96	R = 0.04, T = 0.96
0	20	R = 0.0471, T = 0.9529	Rs = 0.0471, Ts = 0.9529
15	45	R = 0.092, T = 0.9080	Rs = 0.092, Ts = 0.9080

Figure 15 illustrates further the continuity of the RCWA results by generating the reflectance as θ varies from 0 to 90 degrees. Brewster's angle is clearly observed as a *p*-polarized plane wave propagates the air/glass interface. When an incident *s*-polarized plane wave propagates through the system, the reflectance steadily increases as the angle also increases.
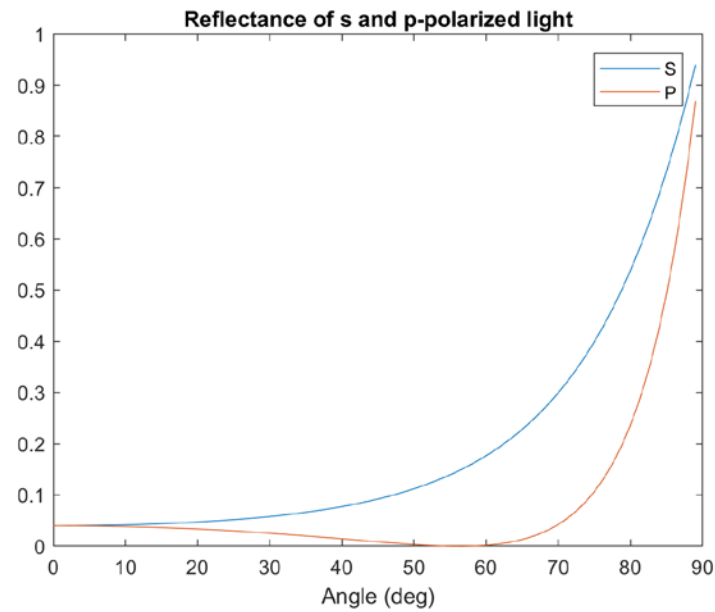
Figure 15 - Reflectance of s and p-polarized light at the air/glass interface generated by RCWA model

5.2. Examining 3D case by applying projection of E-field
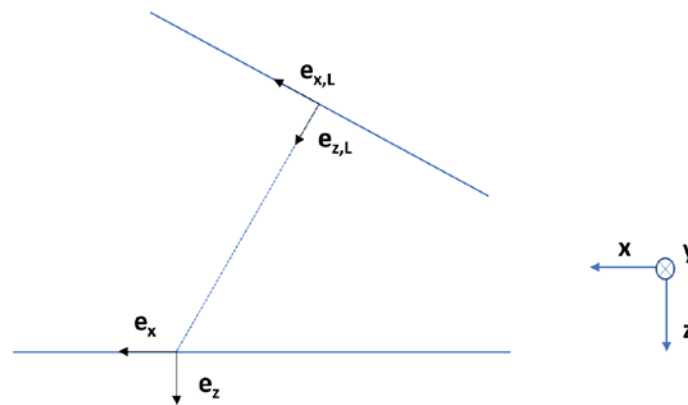
Figure 16 - Setup of E-field projection onto first surface of stack

The projection of the electric field onto the first surface of the system allows the model to

take into account the wave incident at any angle in the three dimensions by incorporating an

optical path difference. The model can then assume the field is propagating in the *z*-direction

within the system.

First, the local coordinates (e_x, e_y, e_z) are defined in terms of the global coordinates ($\hat{e}_x$,

$\hat{e}_y$, $\hat{e}_z$). The z-component of the local and global coordinates are $e_z = (0,0,1)$ and

$\hat{e}_z = k_0(sin\theta cos\phi, sin\theta sin\phi, cos\theta)$, respectively. The *x* and *y*-components of the global

coordinates are determined by the following:

$$\hat{e}_y = \frac{e_z \times k}{|e_z \times k|} \tag{52}$$

$$\hat{e}_x = \hat{e}_y \times \hat{e}_z \tag{53}$$

Therefore, the resulting global coordinates are $\hat{e}_y = (-sin\phi, cos\phi, 0)$ and

$\hat{e}_x = (cos\phi cos\theta, sin\phi cos\theta, -sin\theta)$. Then, the incident E-field is written in terms of the global

coordinates. The matrix used to convert between the local and global coordinates is:

$$\begin{pmatrix} e_x \cdot \hat{e}_x & e_y \cdot \hat{e}_x \\ e_x \cdot \hat{e}_y & e_y \cdot \hat{e}_y \end{pmatrix} = \begin{pmatrix} cos\theta cos\phi & cos\theta sin\phi \\ -sin\phi & cos\phi \end{pmatrix} \tag{54}$$

Then, the optical path difference becomes $OPD = x \sin\theta \cos\phi + y \sin\theta \sin\phi$. The optical path

difference is only utilized if the user desires the model to plot the transmitted and reflected

electric fields in the space domain.

5.3. Testing homogeneous layers [23]
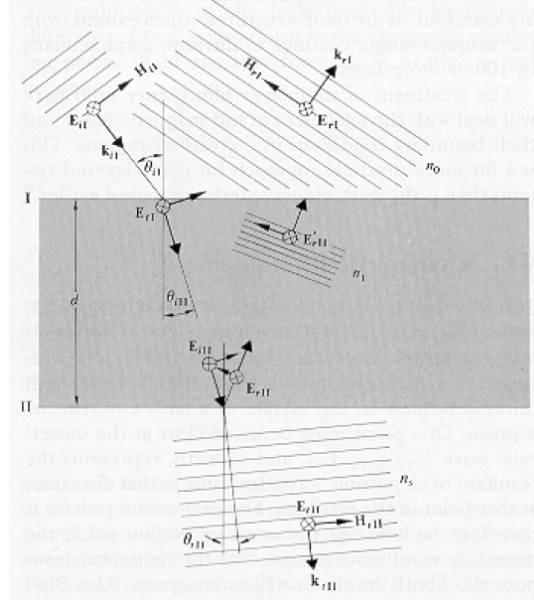
Figure 17 - Electric and magnetic fields in a multilayer film [22]

This test bench is a method of analyzing multilayer thin films. The reflectance and transmittance of a system containing any number of homogeneous layers can be easily determined. The tangential components of **E** and **H** are continuous at each interface. At the first boundary, the relationship between the incident and reflected waves are shown by

$$E_1 = E_{i1} + E_{r1} = E_{t1} + E'_{r2}.$$ (55)

The magnetic field is determined with the following expression:

$$\vec{H} = \sqrt{\frac{\epsilon_0}{\mu_0}} n \vec{k} \times \vec{E}$$ (56)

where the refractive index is defined as $n = \sqrt{\mu \epsilon / \mu_0 \epsilon_0}$. The tangential components of **E** and **H** are continuous at each interface, therefore let us write the following:

$$H_1 = \sqrt{\frac{\epsilon_0}{\mu_0}}(E_{i1} - E_{r1})n_0\cos(\theta_{i1}) = \sqrt{\frac{\epsilon_0}{\mu_0}}(E_{t1} - E'_{r2})n_1\cos(\theta_{i2}) \tag{57}$$

At the second boundary, the electric and magnetic fields are:

$$E_2 = E_{i2} + E_{r2} = E_{t2} \tag{58}$$

$$H_2 = \sqrt{\frac{\epsilon_0}{\mu_0}}(E_{i2} - E_{r2})n_1\cos(\theta_{i2}) = \sqrt{\frac{\epsilon_0}{\mu_0}}E_{t2}n_S\cos(\theta_{t2}) \tag{59}$$

Let us define $k_0(n_1 d\cos(\theta_{i2})) = k_0 h$, $E_{i2} = E_{t1}e^{-ik_0 h}$, and $E_{r2} = E'_{r2} e^{ik_0 h}$. The boundary conditions

at the second boundary are:

$$E_2 = E_{t1}e^{-ik_0 h} + E'_{r2} e^{ik_0 h} \tag{60}$$

$$H_2 = (E_{t1}e^{-ik_0 h} - E'_{r2}e^{ik_0 h})\sqrt{\frac{\mu_0}{\epsilon_0}}n_1\cos(\theta_{i2}) \tag{61}$$

Once E_{t1} and E'_{r2} are solved, their expressions are substituted into Equations (56) and (57) for

the first boundary:

$$E_1 = \frac{1}{\gamma_1}\left(E_2 cos(k_0 h) - H_2(isin(k_0 h))\right) \tag{62}$$

$$H_1 = -E_2\gamma_1 isin(k_0 h) + H_2 cos(k_0 h) \tag{63}$$

where $\gamma_1 = \sqrt{\frac{\epsilon_0}{\mu_0}}n_1\cos(\theta_{i2})$. The above expressions can be summarized in matrix notation:

$$\begin{pmatrix} E_1 \\ H_1 \end{pmatrix} = \begin{pmatrix} cos(k_0 h) & -isin(k_0 h)/\gamma_1 \\ -\gamma_1 isin(k_0 h) & cos(k_0 h) \end{pmatrix}\begin{pmatrix} E_2 \\ H_2 \end{pmatrix} \tag{64}$$

$$\begin{pmatrix} E_1 \\ H_1 \end{pmatrix} = M_1 \begin{pmatrix} E_2 \\ H_2 \end{pmatrix} \tag{65}$$

The matrix $\mathbf{M_1}$ relates the fields at the first boundary. For p layers, the matrices are combined to relate the incident to the outgoing fields:

$$M = M_1 M_2 \cdots M_p = \begin{pmatrix} m_{11} & m_{12} \\ m_{21} & m_{22} \end{pmatrix} \qquad (66)$$

The expression for the reflection and transmission coefficients can be determined. Let us define

$\gamma_0 = \sqrt{\frac{\epsilon_0}{\mu_0}} n_0 \cos(\theta_{i1})$, $\gamma_S = \sqrt{\frac{\epsilon_0}{\mu_0}} n_S \cos(\theta_{t2})$, $r = \frac{E_{r1}}{E_{i1}}$, and $t = \frac{E_{t2}}{E_{i1}}$. Then, Equations 53-57 and 63

are combined to obtain:

$$\begin{pmatrix} E_{i1} + E_{r1} \\ (E_{i1} - E_{r1})\gamma_0 \end{pmatrix} = \begin{pmatrix} m_{11} & m_{12} \\ m_{21} & m_{22} \end{pmatrix} \begin{pmatrix} E_{t2} \\ E_{t2}\gamma_s \end{pmatrix} \qquad (67)$$

The above expression can be rewritten in the form of the following two equations:

$$1 + r = m_{11}t + m_{12}\gamma_s t \qquad (68)$$

$$(1 - r)\gamma_0 = m_{21}t + m_{22}\gamma_s t \qquad (69)$$

Once this system of two equations is solved, the reflection and transmission coefficients are determined:

$$r = \frac{-m_{21} + m_{11}\gamma_0 - m_{22}\gamma_s + m_{12}\gamma_0\gamma_s}{m_{21} + m_{11}\gamma_0 + m_{22}\gamma_s + m_{12}\gamma_0\gamma_s} \qquad (70)$$

$$t = \frac{2\gamma_0}{m_{21} + m_{11}\gamma_0 + m_{22}\gamma_s + m_{12}\gamma_0\gamma_s} \qquad (71)$$

To ultimately find the reflectance and transmittance, the values are squared.

This method can test any number of homogeneous layers and verify against the RCWA model. Table 3 examines the reflectance and transmittance for a system with two, three, and four homogeneous layers, each with 0.1 μm thickness. The incident electric field is not normal to the

system. Table 4 compares the custom RCWA data when modifying the thickness parameter of the final layer. The final thickness parameter can be defined as a discrete distance or as a semi-infinite layer.

Table 3 - Examining reflectance and transmittance for homogeneous layers with 0.1 μm thickness

Homogeneous layers	θ (degrees)	RCWA model	Test bench
Air/Glass/Si	0	R = 0.0923, T = 0.9077	R = 0.0923, T = 0.9077
	20	R = 0.0852, T = 0.9148	R = 0.0852, T = 0.9148
Air/Glass/Si/Al	20	R = 0.5925, T = 0.4075	R = 0.5925, T = 0.4075
Air/Glass/Si/Al/Ti	20	R = 0.7824, T = 0.2176	R = 0.7824, T = 0.2176

Table 4 - Comparing results from custom RCWA model, where the final layer is defined as (A) a semi-infinite layer and (B) a layer with thickness 0.1 μm

Homogeneous layers	θ (degrees)	A	B
Air/Glass/Si	0	R = 0.0923, T = 0.9077	R = 0.5875, T = 0.4125
	20	R = 0.0852, T = 0.9148	R = 0.5979, T = 0.4021
Air/Glass/Si/Al	20	R = 0.5925, T = 0.4075	R = 0.5897, T = 0.4103
Air/Glass/Si/Al/Ti	20	R = 0.7824, T = 0.2176	R = 0.7469, T = 0.2531

The RCWA model is consistent with the results from the Fresnel coefficients and the test bench for multiple homogeneous layers with an incident plane wave at non-normal angles. Now, the RCWA model needs to be tested for the non-homogeneous case, starting with a 1D square grating.

5.4. Fraunhofer diffraction of thin gratings [24]

Fraunhofer diffraction is utilized as a guide for the RCWA and experimental results, which will approximate the diffraction efficiencies of specific orders. For a thin, one-dimensional grating, with a period d along the y_s direction is defined with respect to transmission. The transmission function of the grating inside a circular aperture is:

$$t(x_s, y_s) = \left[f_d(y_s) rect\left(\frac{y_s}{d}\right) * \frac{1}{d} comb\left(\frac{y_s}{d}\right) \right] circ\left(\frac{\sqrt{x_s^2 + y_s^2}}{2a}\right) \tag{72}$$

The transmitted field is expressed as the product of the transmission function and the incident field, $U_s^-(x_s, y_s)$:

$$U_s^+(x_s, y_s) = t(x_s, y_s)U_s^-(x_s, y_s) \tag{73}$$

The incident field is a plane wave propagating through the grating. The diffraction orders are clearly separated provided that the aperture diameter is large compared to the period. Thus, each order can be summed independently. The diffraction efficiency of each order is expressed as:

$$E_m^A = |c_m|^2 \tag{74}$$

where c_m are the Fourier coefficients for a thin grating expressed as the following:

$$c_m = F\left\{ f_d(y_s)\frac{1}{d} rect(\frac{y_s}{d}) \right\}_{\eta=m/d} \tag{75}$$

The Fourier coefficients are rewritten as the convolution of the Fourier transform of each term, $F\{f_d(y_s)\} * F\{rect(y_s / d)/d\}$.

The diffraction efficiencies are determined for each order for any general grating. In the case of a one-dimensional square grating, the function is:

$$f_d(y_s) = rect\left(\frac{y_s}{d/2}\right) \tag{76}$$

This is referred as the binary scalar model. By following Equations (73) and (74), the diffraction efficiency for the square grating is:

$$E_m^A = \left|\frac{1}{2}\,sinc\left(\frac{m}{2}\right)\right|^2 \tag{77}$$

A modified scalar model is used to compare against the experimental results. Rather than a binary square wave, the modified model incorporates a small amount of transmission, shown in the following equations:

$$f_d(y_s) = rect\left(\frac{y_s}{d/2}\right) + \alpha \tag{78}$$

where α corresponds to a small constant. The Fourier coefficients become:

$$\begin{aligned} c_m &= F\left\{\frac{1}{d}rect\left(\frac{y_s}{d/2}\right) + \frac{\alpha}{d}rect\left(\frac{y_s}{d}\right)\right\}_{\eta=m/d} \\ &= \frac{1}{2}sinc\left(\frac{m}{2}\right) + \alpha\,sinc(m) \end{aligned} \tag{79}$$

The offset value α utilized is set to 0.262.

Table 5 summarizes the diffraction efficiencies of the 1D square gratings for the two scalar models. The table is a guide to gauge the accuracy of the simulated and experimental results.

Table 5 - Diffraction efficiencies of diffraction orders for 1D square grating

Models	0	± 1	± 2	± 3
Binary scalar	0.25	0.101	0	0.011
Modified scalar	0.37	0.08044	0.01658	0.0003

As the duty cycle increases, the transmitted efficiency of the modified scalar model also increases. Figure 18 is used as reference for the theoretical model, since the tested grating will not have a 50% duty cycle.
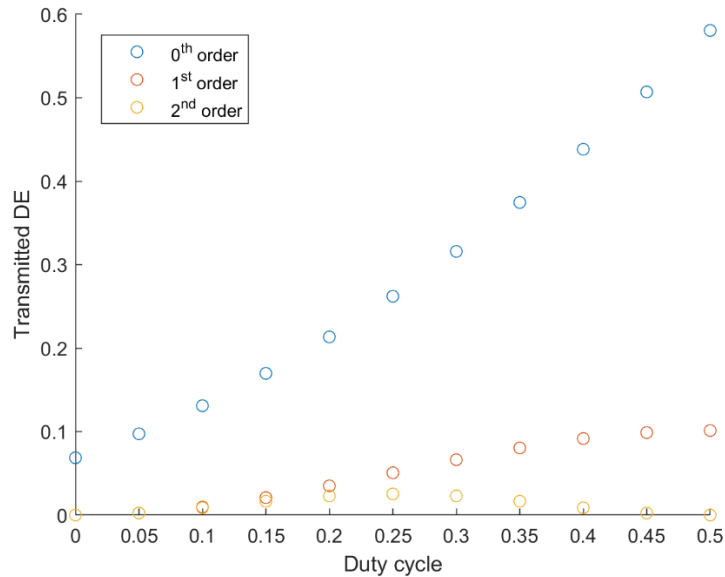
Figure 18 - Diffraction efficiency of modified scalar model as duty cycle varies

5.5. Examining the 1D square grating under SEM

As shown in Figure 19, the 1D square grating used experimentally was examined under the single electron microscope to verify the duty cycle and period. The back-scattered images from the scanning electron microscope are extracted to observe the structure of the glass and chromium surfaces. The SEM effectively liberates the surface electrons to emit a back-scattered image of the sample. Since glass contains more surface electrons than chromium, the lighter sections correspond to the glass substrate in contrast to the darker sections, which are the chromium deposits. At a glance, the duty cycle of the grating is clearly not equal to 50%. Upon closer examination, the duty cycle of this grating is 36%. This measurement will be considered for the simulations, since this will highly influence the transmitted and reflected diffraction

efficiencies. The period matches the specifications listed in the Edmund Optics catalogue, 6.6 μm.
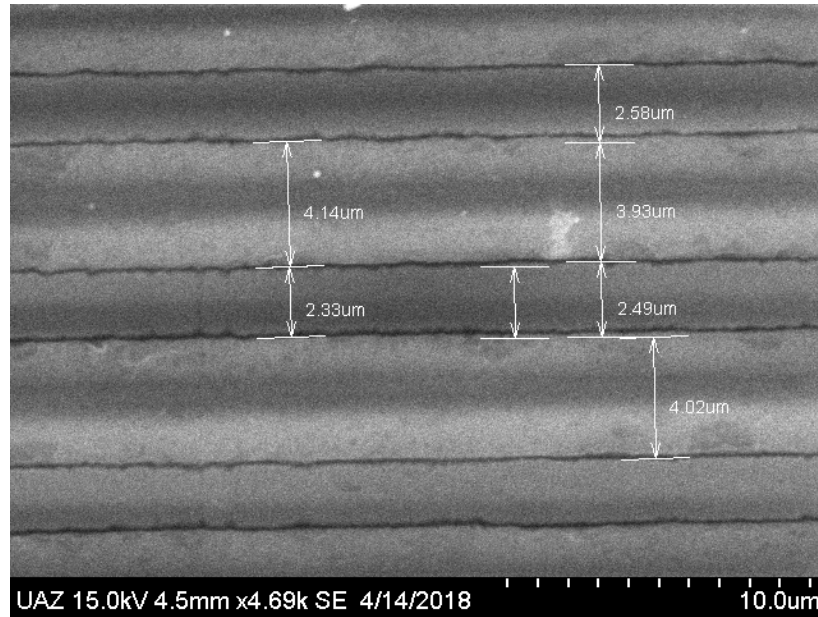
Figure 19 - SEM image of glass/chromium grating

5.6. Experimental results of 1D square grating
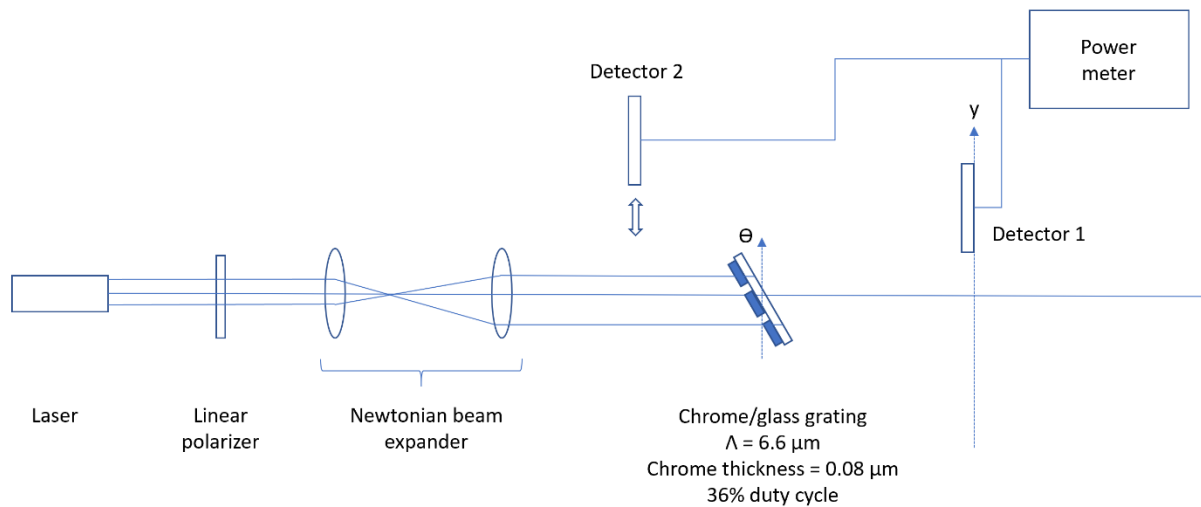
Figure 20 - Experimental setup

The setup, shown in Figure 20, examines the diffraction efficiency of a 1D square grating, composed of chrome and glass with a period of 6.6 μm. The chrome thickness is 0.08 μm [25], while the entire grating has a thickness of approximately 1.1 mm. A tunable, high powered supercontinuum Fianium laser emits a white light. The wavelength is modified with the aid of a filter. Then, a linear polarizer controls the polarization of the field to either *s* or *p* polarizations. The light propagates through a beam expander, which increases the diameter of the beam by two. The final beam propagates onto the grating and detects the emitted power from the PM320E dual channel benchtop power meter. In order to find the transmitted diffraction efficiency, the power from detector 1 is measured. Next, the second detector comes down into the beam path and is also observed. The diffraction efficiency is the fraction of power from detector 1 and power from detector 2. The Fresnel losses from the glass are additionally regarded as part of the final calculation of the transmitted efficiency.

First, the diffraction efficiency is observed when the grating is set at normal incidence. In other words, the grating is oriented perpendicular to the optical axis. In Figure 21, these experimental results are compared against the scalar and modified scalar models. Note, both the scalar model and modified scalar models correspond to a duty cycle near 36%. The small amount of transmission in the modified scalar model corresponds to the transmission through the chromium deposits. Overall, the experimental data and the modified scalar model roughly matches.
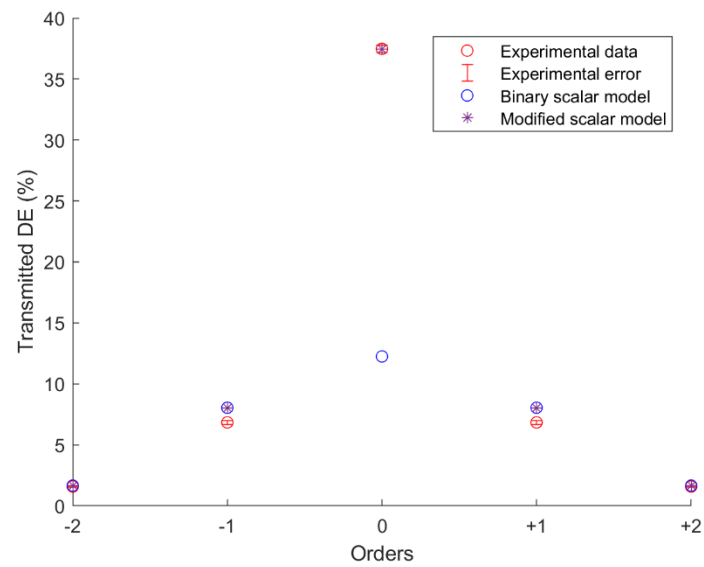
Figure 21 - Comparison between experimental data and scalar models for grating oriented perpendicular to the OA

Second, the transmitted diffraction efficiency was observed as the rotation angle of the grating changed. The experimental data was compared directly against the OptiScan RCWA model. Overall, this theoretical model closely matches the experimental data. RCWA does not consider Fresnel losses from the first surface, which explains the small deviations between the two. The experimental results will then be compared against the other two models, Polaris-M and Matlab.
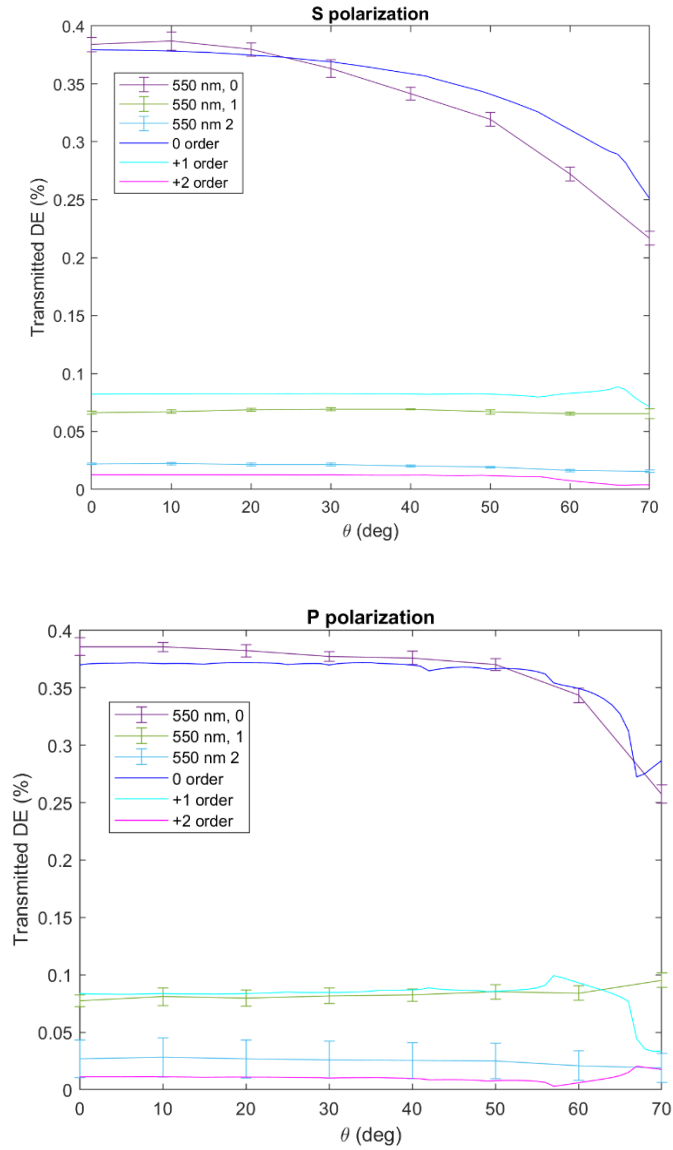
Figure 22 - Comparison between experimental results, shown with error bars, and OptiScan RCWA model for (a) s polarized light and (b) p polarized field

5.7. Polaris-M's RCWA model

The Polaris-M RCWA model closely matches the experimental results. Figure 23 illustrates the transmitted diffraction efficiency of the 1D square grating as the rotational angle increases. In the Polaris-M model, the grating is initialized with 36% duty cycle as shown in Section 5.5. The Fresnel losses from the second surface are included in the Polaris-M calculations.
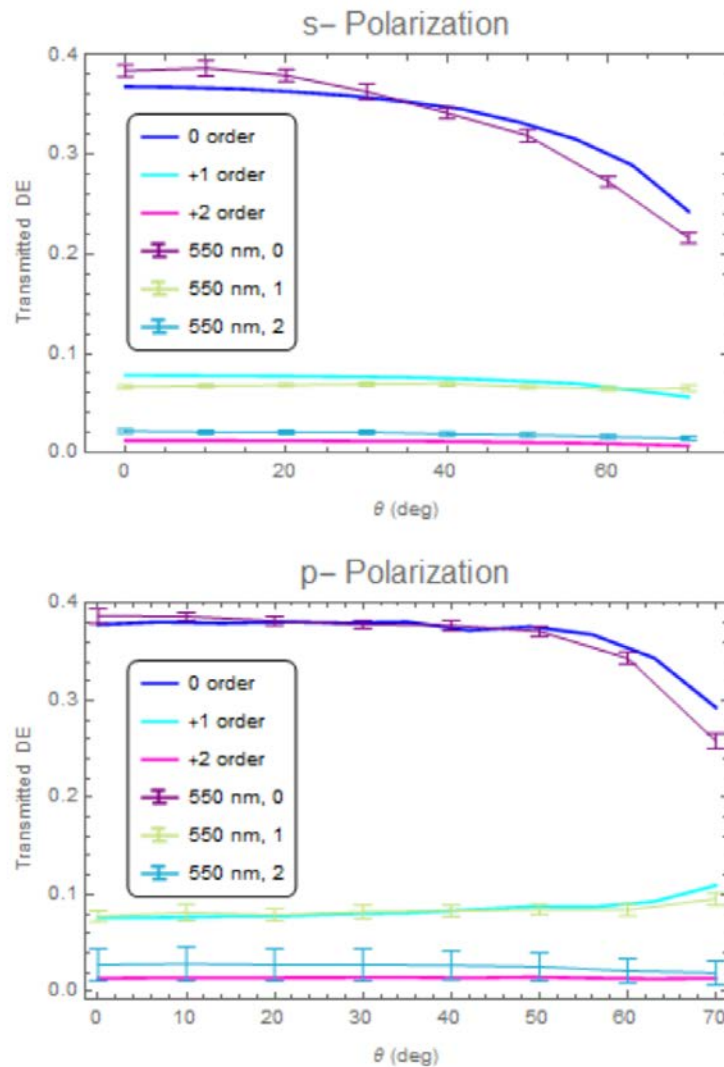
Figure 23 - Comparison between experimental data, shown with error bars, and Polaris-M RCWA model

5.8. RCWA Matlab simulations

The RCWA Matlab model clearly needs to be improved. In Figure 25, the transmitted diffraction efficiency largely deviates from the experimental data. The diffraction efficiency at normal incidence for the 0th order is approximately 27%, rather than the 38% observed experimentally. The run time of the Matlab model also needs to be optimize. In order to look at

the first three orders, 85 Fourier coefficients need to be initialized, which significantly increases the run time. In addition, the numerical noise needs to be improved as demonstrated in Figure 26.
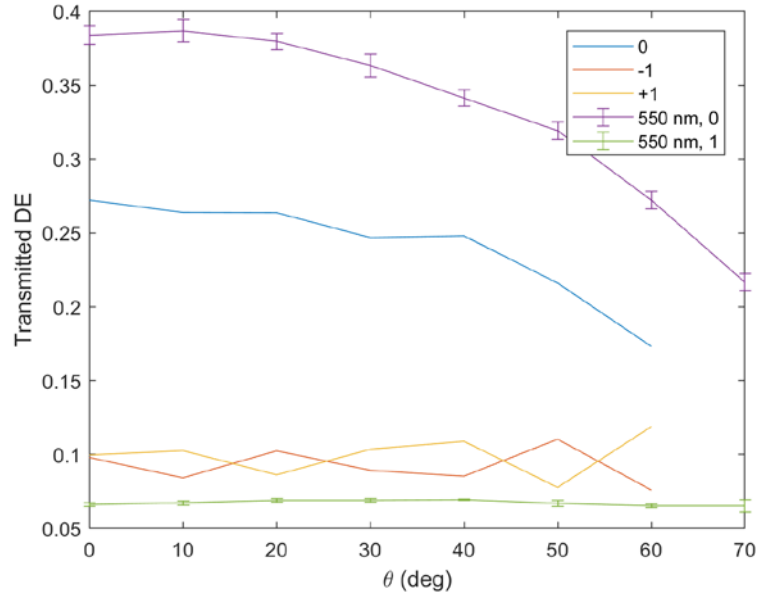
Figure 24 - Comparison between Matlab RCWA and experimental data, shown with error bars, for s-polarized light
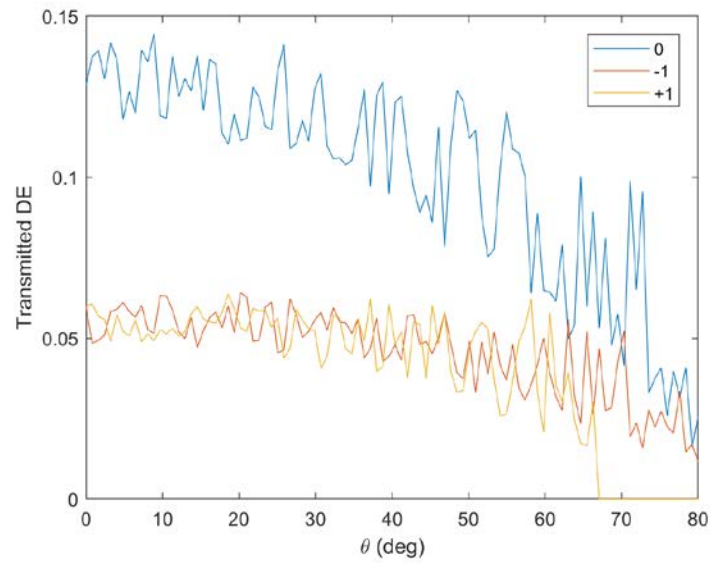
Figure 25 - Varying rotation angle of grating for 1D square grating with 50% duty cycle

Chapter 6 – Rayleigh Anomalies and Non-paraxial Scalar Diffraction Theory

6.1. Non-paraxial Scalar Diffraction Theory [14]

The Fresnel and Fraunhofer approximations are only proven to be valid in the paraxial limitation. In other words, these theories are only valid with small diffraction angles and small angles of incidence, which corresponds to the $\lambda/d < 0.1$ case for gratings. However, Harvey argues that scalar diffraction theory can remain valid in the non-paraxial case. Since the diffracted radiance is shift invariant in the direction cosine space, Fourier techniques can predict wide-angle diffraction grating effects.
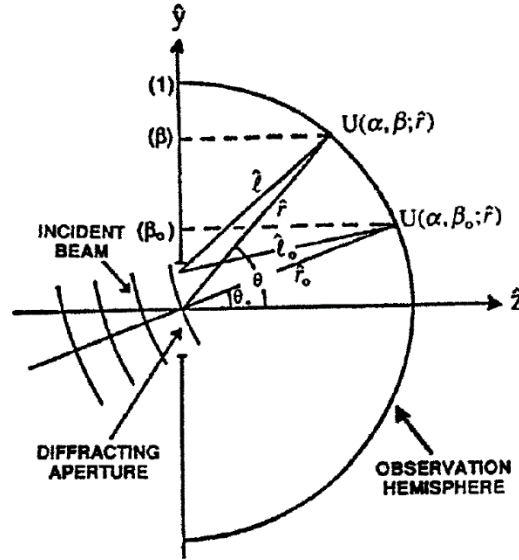
Figure 26 - Configuration of the incident beam, the diffracting aperture, and the observation hemisphere [13]

In the Fraunhofer region, i.e. far field, the paraxial irradiance distribution is the modulus squared of the field after propagating through the aperture.

$$E(x_2, y_2) = \frac{E_0}{\lambda^2 z^2}\left| F\left\{U_0^+(x_1, y_1)\right\}_{\xi=\frac{x_2}{\lambda z}, \eta=\frac{y_2}{\lambda z}} \right|^2 \tag{80}$$

The field propagating through the aperture is defined in terms of the aperture function and the incident field as shown in Equation (73).

First, the spatial variables would be normalized by the wavelength of the incident light:

$$\hat{x} = x/\lambda, \ \hat{y} = y/\lambda, \ \hat{z} = z/\lambda \tag{81}$$

The reciprocal variables in the Fourier domain become the direction cosines of the propagation vectors of the plane wave.

$$\alpha = \hat{x}/\hat{r}, \ \beta = \hat{y}/\hat{r}, \ \gamma = \hat{z}/\hat{r} \tag{82}$$

Since radiance is expressed in units of power per unit area, the diffracted radiance becomes:

$$L'(\alpha, \beta - \beta_0) = K \frac{\lambda^2}{A_s} \left| F\left\{ U'_0(\hat{x}, \hat{y}; 0) e^{i2\pi\beta_0 \hat{y}} \right\} \right|^2 \ \text{for} \ \alpha^2 + \beta^2 \leq 1 \tag{83}$$

$$L'(\alpha, \beta - \beta_0) = 0 \ \text{for} \ \alpha^2 + \beta^2 > 1$$

Where the renormalization factor is defined as:

$$K = \frac{\int_{\alpha=-\infty}^{\infty} \int_{\beta=-\infty}^{\infty} L(\alpha, \beta - \beta_0) d\alpha d\beta}{\int_{\alpha=-1}^{1} \int_{\beta=-\sqrt{1-\alpha^2}}^{\sqrt{1-\alpha^2}} L(\alpha, \beta - \beta_0) d\alpha d\beta} \tag{84}$$

This factor will only deviate from unity only if evanescent waves are produced, which is the key component to predicting Rayleigh anomalies.

6.2. Experimental observation of Rayleigh anomalies

Rayleigh anomalies are characterized by a sharp increase in the diffraction efficiency as an order becomes evanescent. As the grating is rotated, the transmitted orders one by one become evanescent. Once this occurs, then the increase of the diffraction efficiency of the neighboring orders should be observed.
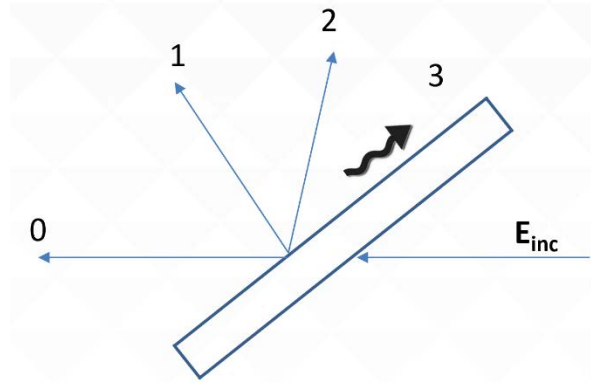
Figure 27 - Illustration of diffraction orders from a grating, where the third order becomes evanescent

6.3. Rayleigh anomalies for 1D square grating

The characterization of the efficiency behavior is done by setting the grating such that it satisfies the Littrow condition for a specific diffracted order. For transmission gratings, a given diffracted order satisfies the Littrow condition if $\theta_m = -\theta_i$, as shown in Figure 29. It is more common to examine the Littrow condition for a reflection grating, where $\theta_m = \theta_i$. The position of the source and detector remain unchanged. The grating angle is the only varying parameter.
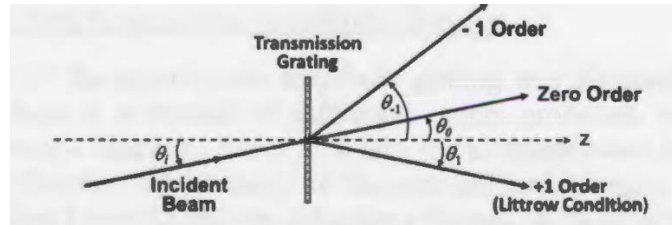
Figure 28 - Setup for a transmission diffraction grating to satisfy the Littrow condition [14]

If the +1 diffracted order satisfies the Littrow condition, then the grating equation results in the expression below for the incident angle:

$$\theta_i = sin^{-1}(0.5\lambda / d) \tag{85}$$

Where d represents the grating period and λ is the wavelength of the incident field. Equation (83) can be rearranged to the following expression:

$$sin\theta_m = \left(\frac{1}{2} - m\right)\frac{\lambda}{d}$$

(86)

The +1 and -1 orders produced by a transmission grating propagate at the angles:

$$\theta_1 = -sin^{-1}\left(\frac{1}{2}\frac{\lambda}{d}\right) \text{ and } \theta_{-1} = sin^{-1}\left(\frac{3}{2}\frac{\lambda}{d}\right)$$

(87)

As the rotational angle of the grating increases, λ/d also increases. As shown in Table 6, we observed the angles at which the orders of the chrome/glass grating became evanescent with the corresponding λ/d values.

Table 6 - Angles at which the orders for the chrome/glass grating become evanescent

Evanescent orders	Θ (deg)	$(\lambda/d)_{+1}$	$(\lambda/d)_{-1}$
5	32	1.0598	0.3533
4	39	1.2586	0.4195
3	46	1.4387	0.4796
2	54	1.618	0.5393
1	66	1.8271	0.6090

6.4. Design of a new grating holder

The grating holder is a possible source of error for these experiments. Parts of the previous grating holder were impeding the transmitted beam, which could possibly lead to inaccurate results. The goal of designing this holder is to capture all of the transmitted beams.
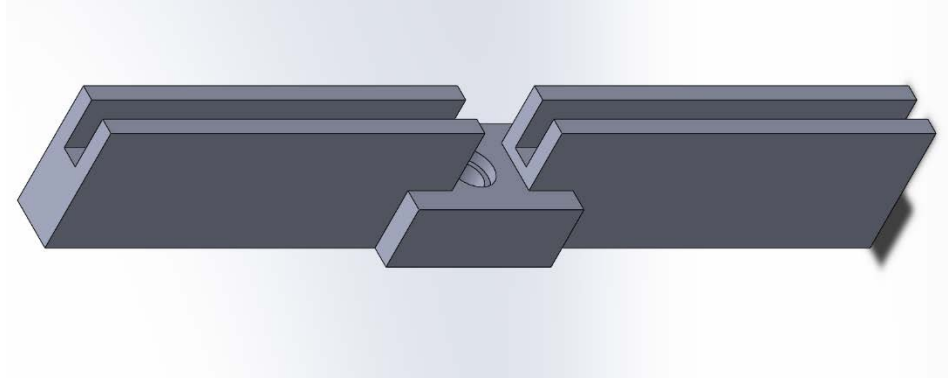
Figure 29 - Design of a grating holder to avoid blocking the transmitted beams

6.5. Results

The grating was rotated to observe the Rayleigh anomalies as a function of the transmission diffraction efficiency. When the grating is rotated, orders become evanescent. These angles are noted to compare to the results, shown in Table 6, which deviate from the results in Figure 6. Once an order becomes evanescent, then a small increase in the diffraction efficiency should be observed. However, Figure 31 demonstrates that this is not the case. Figures 32 and 33 compare the diffraction efficiencies between the OptiScan and experimental data. Based off of these experimental results, the validation of the non-paraxial scalar diffraction theory remains inconclusive.
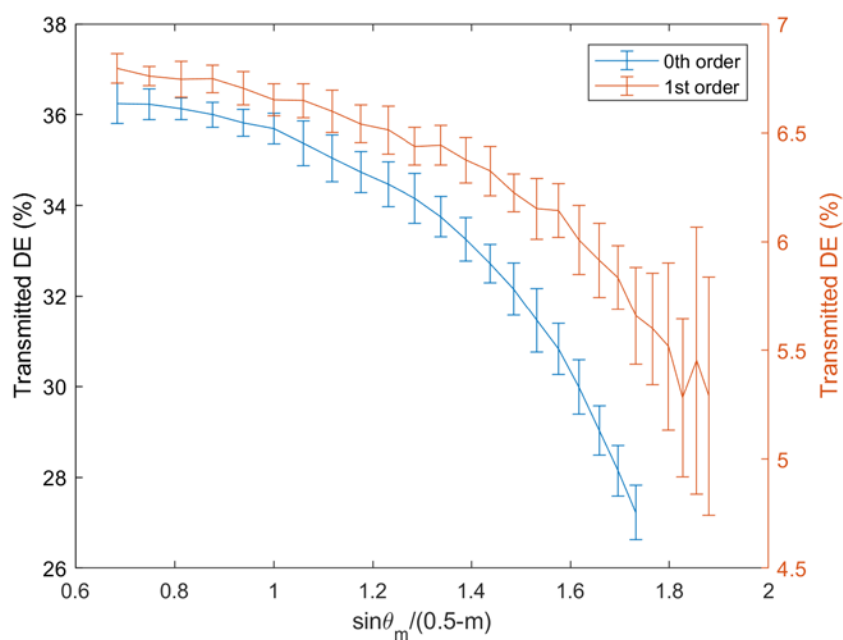
Figure 30 - Transmission diffraction efficiency as rotational angle of grating changes
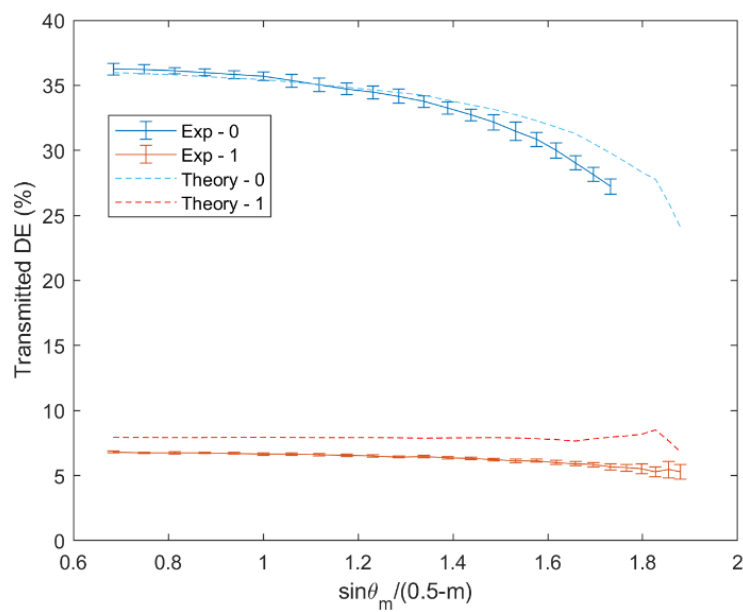
Figure 31 - Comparison between experimental and OptiScan data of the 0th and 1st orders
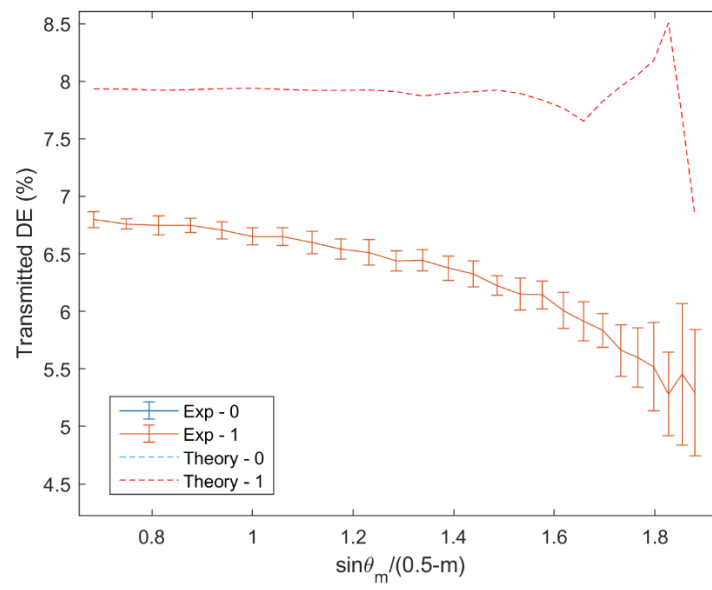
Figure 32 - Close up comparison of the 1st order from Figure 31

Chapter 7 – Summary and Conclusion

A user-friendly RCWA model was developed in Matlab. A verification process was followed to validate and determine the limitations of the model. The model was first tested against simple cases: air/glass interface and multiple homogeneous layers. Then, it was tested against the simplest non-homogeneous case, a 1D square grating. The experimental data was compared against three theoretical, RCWA models: OptiScan, Polaris-M, and Matlab. Originally, the models assumed a 1D square grating with a 50% duty cycle. Since there was a discrepancy between the theoretical models and the experimental data, the grating used experimentally was observed under the single electron microscope. The grating was shown to have a 36% duty cycle, rather than a 50% duty cycle. Then, it was shown that the OptiScan and Polaris-M results aligned with the experimental ones.

Further work needs to be done to understand the results from the Matlab RCWA model. The primary noted limitations of the Matlab RCWA model are the numerical noise and the total run time. The large deviations between the Matlab RCWA model and the experimental results need to be discerned. The convergence of the diffraction efficiencies as the number of Fourier coefficients increases would need to be examined.

Harvey observed Rayleigh anomalies when applying the non-paraxial diffraction model. However, the experiments do not demonstrate these anomalies. The primary difference between this model and the experimental results is the overall trend. Harvey's model illustrates a constant trend with sharp increases of the efficiency corresponding to the anomalies. The experimental results show a downward trend due to the Fresnel losses through the materials. The model does not take this into account. Therefore, the verification of the non-paraxial scalar diffraction model remains inconclusive.

Appendix A

Raw Experimental Data

Data of grating at normal incidence

$\lambda = 450$ nm

Orders	Measured Power (µW)	Reference power (µW)
0	16.5, 38, 28.8, 30.3, 22.7	43, 97, 73, 78, 58
1	3.1, 6.8, 5.2, 5.5, 4.2	42, 97, 74, 77, 57
2	.57, 1.46, 1.2, 1.1, 1.1	41, 97, 74, 76, 58

$\lambda = 550$ nm

Orders	Measured Power (µW)	Reference power (µW)
0	51, 60, 39, 41, 45	132, 152, 100, 105, 115
1	9.5, 11.1, 7, 7.6, 8.3	135, 153, 99, 105, 115
2	2.28, 2.5, 1.7, 1.8, 1.96	135, 154, 99, 106, 116

$\lambda = 650$ nm

Orders	Measured Power (µW)	Reference power (µW)
0	59, 59, 40.9, 43.5, 70.8	151, 153, 105, 116, 180
1	10.9, 11, 7.6, 8.7, 12.5	151, 152.6, 105, 116, 181
2	2.55, 2.58, 1.78, 1.9, 2.97	151, 153, 105.6, 116, 180

Data of grating at varying rotational angles

450 nm and s polarization

Θ (deg)	Orders	Measured Power (μW)	Reference Power (μW)
0	0	46, 43, 37, 40.5, 24	112, 102, 89, 97, 57
	1	7.9, 7.4, 6.6, 6.8, 4.6	111, 100, 89, 92, 56
	2	2.7, 2.7, 2.5, 2.6, 1.98	111, 101, 88, 94, 56
10	0	46, 44, 37, 41, 24	112, 102, 90, 97, 56
	1	8.2, 7.4, 6.6, 7, 4.6	112, 103, 89, 94, 56
	2	2.9, 2.8, 2.7, 2.7, 1.97	111, 103, 89, 94, 56
20	0	45, 43, 36.9, 40, 24	112, 103, 90, 96, 56
	1	8.2, 7.5, 6.8, 7, 4.8	111, 101, 89, 94, 56
	2	2.9, 2.9, 2.7, 2.8, 2	111, 100, 89, 94, 56
30	0	43, 41, 34.8, 38, 22.9	111, 100, 90, 96, 56
	1	8.2, 7.7, 6.8, 7.1, 4.7	112, 100, 90, 94, 56
	2	2.7, 2.6, 2.4, 2.5, 1.9	111, 103, 88, 94, 56
40	0	41, 39, 33, 35.5, 21.5	111, 99, 89, 95, 56
	1	8.2, 7.6, 6.8, 7.1, 4.7	111, 99, 89, 93, 56
	2	2.5, 2.5, 2.3, 2.4, 1.9	111, 102, 89, 94, 56
50	0	39, 35, 30.7, 32, 20	111, 101, 89, 94, 57
	1	8.1, 7.4, 6.6, 6.9, 4.5	111, 100, 89, 94, 56
	2	2.57, 2.4, 2.2, 2.4, 1.8	111, 99, 89, 94, 56
60	0	32, 30, 26, 27, 16.8	111, 103, 89, 94, 56
	1	7.9, 7.1, 6.3, 6.8, 4.4	111, 100, 89, 94, 55
	2	2.2, 2.2, 2, 2.2, 1.6	111, 104, 89, 94, 56
70	0	26, 23, 20, 21, 13	112, 102, 90, 94, 56
	1	6.8, 6.9, 6, 6.3, 4.4	111, 101, 88, 94, 56
	2	1.9, 2.2, 1.9, 2.06, 1.4	111, 101, 89, 94, 56

450 nm and p polarization

Θ (deg)	Orders	Measured Power (µW)	Reference Power (µW)
0	0	22, 21.5, 17.3, 10.9, 14	54, 51, 43, 25, 32
	1	4.2, 4.1, 3.6, 2.6, 3.1	53, 51, 42, 25, 32
	2	1.8, 1.7, 1.7, 1.4, 1.6	53, 50, 41, 25, 32
10	0	22, 21.5, 17.6, 10.9, 14	54, 49, 42, 25, 33
	1	4.3, 4, 3.7, 2.7, 3.1	53, 50, 42, 25, 32
	2	1.9, 1.8, 1.8, 1.4, 1.55	52, 48, 41, 25, 32
20	0	21.7, 21, 17.4, 10.7, 13.9	54, 51, 42, 25, 32
	1	4.4, 4.2, 3.8, 2.7, 3.1	52, 49, 41, 24, 33
	2	1.7, 1.8, 1.7, 1.4, 1.5	52, 50, 41, 25, 32
30	0	21.4, 20.8, 17, 10.7, 13.6	54, 51, 42, 25, 33
	1	4.4, 4.3, 3.7, 2.7, 3.2	53, 51, 41, 26, 32
	2	1.7, 1.7, 1.6, 1.35, 1.5	52, 50, 41, 25, 32
40	0	20.7, 20, 16.8, 10.5, 13.5	53, 51, 42, 25, 33
	1	4.5, 4.4, 3.8, 2.7, 3.3	53, 50, 41, 26, 32
	2	1.6, 1.6, 1.5, 1.3, 1.48	51, 49, 41, 25, 32
50	0	20.7, 19.8, 16.5, 10.3, 13.4	53, 49, 42, 26, 32
	1	4.6, 4.5, 3.9, 2.8, 3.3	53, 49, 42, 25, 32
	2	1.6, 1.6, 1.5, 1.3, 1.4	52, 49, 40, 25, 32
60	0	19, 19, 15.9, 9.7, 12.5	53, 51, 42, 26, 32
	1	4.7, 4.6, 4, 2.8, 3.3	52, 51, 41, 25, 32
	2	1.45, 1.5, 1.4, 1.2, 1.3	52, 49, 41, 25, 32
70	0	16.4, 15.8, 12.7, 8.3, 9.9	53, 51, 43, 25, 33
	1	4.9, 4.9, 4.1, 2.8, 3.5	52, 49, 41, 25, 32
	2	1.2, 1.3, 1.2, 1, 1.1	52, 49, 40, 25, 32

550 nm and s polarization

Θ (deg)	Orders	Measured Power (μW)	Reference Power (μW)
0	0	44, 41, 48, 39, 34.5	108, 104, 120, 97, 86
	1	7.6, 7.3, 8.2, 6.6, 6	109, 104, 122, 96, 86
	2	2.5, 2.4, 2.7, 2.1, 2	109, 104, 123, 93, 84
10	0	43, 41, 49, 39.7, 34.9	107, 104, 120, 97, 86
	1	7.7, 7.5, 8.3, 6.7, 6.1	110, 104, 122, 97, 86
	2	2.4, 2.4, 2.8, 2.2, 2.1	108, 104, 123, 94, 84.5
20	0	42, 41, 48, 39, 34.5	108, 104, 121, 98, 86
	1	7.99, 7.6, 8.6, 6.8, 6	110, 104, 121, 95, 86
	2	2.3, 2.3, 2.7, 2.1, 2	108, 103, 124, 93, 85
30	0	41, 38, 46, 37, 33	107, 104, 121, 97, 86
	1	8, 7.6, 8.6, 6.8, 6.2	109, 105, 122, 94, 85
	2	2.27, 2.2, 2.6, 2.1, 2	108, 103, 124, 92, 85
40	0	39, 36, 43, 35, 31	109, 104, 120, 97, 87
	1	7.8, 7.6, 8.6, 6.8, 6.1	109, 104, 120, 94, 85
	2	2.27, 2.24, 2.5, 1.9, 1.9	107, 103, 122, 92, 84.5
50	0	37, 34, 41, 32, 28.8	109, 104, 121, 98, 87
	1	7.5, 7.3, 8.2, 6.7, 6.1	108, 104, 122, 95, 85
	2	2.14, 2.2, 2.35, 1.8, 1.7	107, 103, 124, 92, 85
60	0	31, 30.6, 34, 27, 24	110, 104, 120, 96, 86
	1	7.6, 7, 8.2, 6.6, 5.8	109, 104, 122, 94, 85
	2	1.7, 1.8, 2, 1.6, 1.5	107, 103, 123, 90, 85
70	0	25.6, 24, 27, 21, 19.4	110, 104, 122, 96, 86
	1	7.1, 6.6, 8.9, 6.6, 5.8	109, 104, 122, 93, 85
	2	1.85, 1.66, 1.9, 1.6, 1.4	108, 103, 124, 91, 85

550 nm and p polarization

Θ (deg)	Orders	Measured Power (μW)	Reference Power (μW)
0	0	9.1, 18, 14, 9.8, 17.7	22, 46, 35, 24, 44

	1	1.9, 3.4, 2.7, 2, 3.3	21.7, 45, 34, 23.8, 43.5
	2	0.859, 1.2, 1.1, 0.92, 1.2	21.5, 45, 33, 23, 43
10	0	8.8, 18.3, 14, 9.8, 17.7	22, 46, 35, 24, 44
	1	2, 3.4, 2.8, 2.1, 3.4	21.3, 45, 34, 23, 43
	2	0.857, 1.3, 1.13, 0.99, 1.3	21, 44, 32, 23.5, 42
20	0	8.8, 18, 13.9, 9.7, 17.6	22, 46, 35, 24, 44
	1	1.97, 3.4, 2.8, 2.1, 3.3	21.5, 45, 34, 23.7, 43
	2	0.845, 1.2, 1.07, 0.91, 1.3	21, 44, 33, 23, 42
30	0	8.6, 18, 13.8, 9.6, 17.2	22, 46, 35, 24, 44
	1	2, 3.6, 2.8, 2.1, 3.4	21.3, 45, 34, 23, 43
	2	0.825, 1.2, 1.03, 0.9, 1.2	21, 44, 33, 23, 42
40	0	8.7, 17.4, 13.5, 9.5, 17	21.7, 45, 35, 24, 44
	1	2, 3.6, 2.9, 2.1, 3.5	21.5, 45, 33.7, 23.7, 43
	2	0.790, 1.16, 0.998, 0.87, 1.1	21, 45, 33, 23, 42
50	0	8.4, 18, 13.3, 9.4, 16.8	21.8, 46, 35, 24, 44
	1	2.1, 3.7, 2.9, 2.2, 3.6	21.5, 45, 34, 23.7, 42
	2	0.770, 1.17, 0.96, 0.86, 1.1	21, 45, 32, 23, 42
60	0	7.9, 16, 12.5, 8.7, 15.7	21.7, 46, 35, 24, 44
	1	2.03, 3.7, 2.9, 2.2, 3.5	21.4, 45, 33.5, 23.7, 43
	2	0.613, 0.94, 0.83, 0.73, 0.9	21, 45, 32.5, 23, 42
70	0	6, 12, 9.3, 6.5, 11.4	21.6, 46, 35, 24, 43.5
	1	2.25, 4.2, 3.2, 2.5, 4	21.5, 45, 33.5, 23.5, 43
	2	0.565, 0.83, 0.67, 0.76, 0.79	21, 45, 32, 23, 42

650 nm and s polarization

Θ (deg)	Orders	Measured Power (μW)	Reference Power (μW)
0	0	44.8, 38, 37, 40, 56.7	112, 96, 93, 98, 140
	1	7.5, 6.5, 6.4, 6.6, 9.5	112, 95.5, 94, 98, 142
	2	2.27, 2, 1.98, 2.1, 2.9	112, 96, 94, 99, 141

| 10 | 0 | 45, 38.5, 37.8, 40.7, 56.8 | 113, 95.5, 94, 102, 142 |
	1	7.66, 6.6, 6.5, 6.9, 9.6	112, 95.7, 95, 99, 141
	2	2.3, 2, 2.1, 2.15, 3	112, 95.5, 94, 98, 141
20	0	44.7, 38, 37, 39.8, 56	112, 96, 94, 101, 142
	1	7.6, 6.7, 6.45, 6.9, 9.7	112, 95.5, 95, 100, 141
	2	2.3, 2.07, 2.07, 2.2, 3	112, 96, 94, 98, 141
30	0	42.5, 36, 36, 38, 53.7	112, 95.5, 94, 100, 141
	1	7.8, 6.8, 6.7, 7, 9.8	112, 96, 94, 100, 142
	2	2.3, 1.97, 2, 2.1, 2.9	111, 95.7, 94, 98, 140
40	0	40, 34, 34, 35.5, 50.8	111, 96, 94, 99, 142
	1	7.9, 6.8, 6.6, 6.9, 9.8	112, 96, 93, 100, 142
	2	2.16, 1.9, 1.9, 2, 2.7	111, 96, 94, 98, 141
50	0	37.5, 32, 31, 32, 46.7	111, 95.5, 94, 98, 141
	1	7.7, 6.6, 6.6, 7, 9.6	112, 96, 95, 99, 141
	2	2.05, 1.89, 1.85, 1.9, 2.6	111, 96, 94, 98, 141
60	0	31.4, 26.8, 26.5, 27, 39.5	111, 95.7, 95, 98, 141
	1	7.3, 6.6, 6.5, 6.6, 9.7	111, 95.5, 95, 99, 141
	2	1.8, 1.7, 1.6, 1.7, 2.2	111, 96, 94, 99, 141
70	0	24.8, 21.2, 21, 20, 30.8	112, 95.8, 94, 98, 141
	1	7.56, 6.2, 6.2, 6.3, 8.9	111, 95.5, 94, 99, 141
	2	1.6, 1.6, 1.2, 1.5, 2.2	111, 96, 93, 99, 141

650 nm and p polarization

Ө (deg)	Orders	Measured Power (µW)	Reference Power (µW)
0	0	35, 32.6, 27, 37, 31	91, 82.5, 69, 94, 79
	1	6.3, 5.5, 4.9, 6.5, 5.6	90, 80, 69, 94, 79
	2	1.9, 1.7, 1.5, 2, 1.7	89, 79, 66, 92, 79
10	0	35.5, 32.6, 27, 37.4, 31.5	90, 82.5, 69, 94, 80
	1	6.3, 5.6, 4.9, 6.5, 5.7	90, 80, 69, 93, 80

	2	2, 1.8, 1.54, 2, 1.8	89, 79, 66, 92, 80
20	0	35.4, 32.3, 27, 37, 31	90, 82, 68, 94, 79
	1	6.4, 5.7, 5, 6.7, 5.8	90, 80, 68, 94, 80
	2	1.9, 1.8, 1.5, 2, 1.8	89, 79, 66, 92.8, 80
30	0	35, 31.7, 26.8, 36.8, 30	90, 83, 69, 94, 79
	1	6.6, 5.8, 5.1, 6.8, 5.9	90, 80, 69, 93.5, 80
	2	1.8, 1.6, 1.4, 1.9, 1.7	89, 79, 65, 92, 80
40	0	34, 30.9, 26, 35.8, 30	90, 81, 68, 94, 79
	1	6.9, 6, 5.3, 7.1, 6.7	89, 79.7, 69, 93, 79
	2	1.7, 1.6, 1.4, 1.8, 1.6	88, 79, 66, 92, 80
50	0	34.8, 31, 26.5, 35.9, 30	90, 81, 69, 94, 79
	1	6.8, 6, 5.2, 7, 6	89, 79, 68, 93, 80
	2	1.66, 1.5, 1.3, 1.7, 1.5	89, 78, 65, 92, 79
60	0	31, 28, 24, 32.7, 27	90, 81, 69, 94, 79
	1	7, 6.3, 5.18, 7.3, 6.3	89, 79, 68, 93, 80
	2	1.36, 1.3, 1.1, 1.4, 1.3	88, 79, 65, 92, 79
70	0	25.9, 23, 19.8, 27, 22.5	89, 81, 69, 94, 79
	1	7.8, 6.9, 5.8, 8, 6.9	89, 79, 66, 93, 80
	2	1.3, 1.3, 1.16, 1.5, 1.3	88, 79, 65, 92, 80

Appendix B

Additional Experimental Results
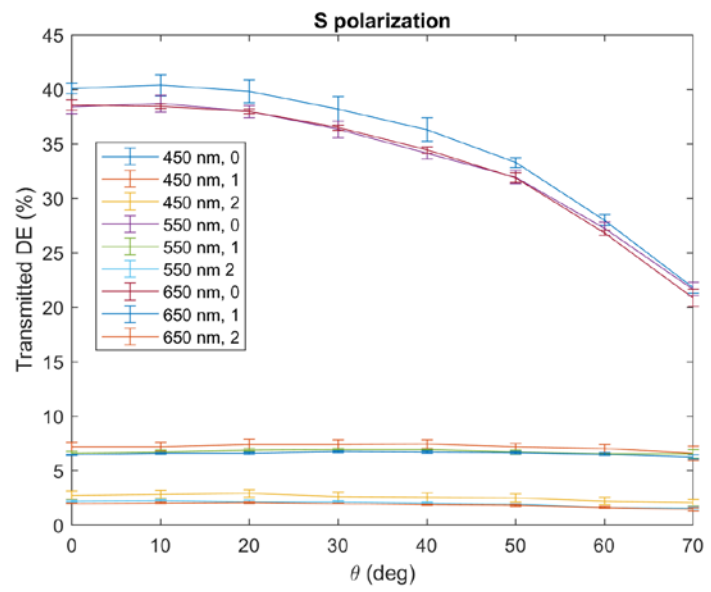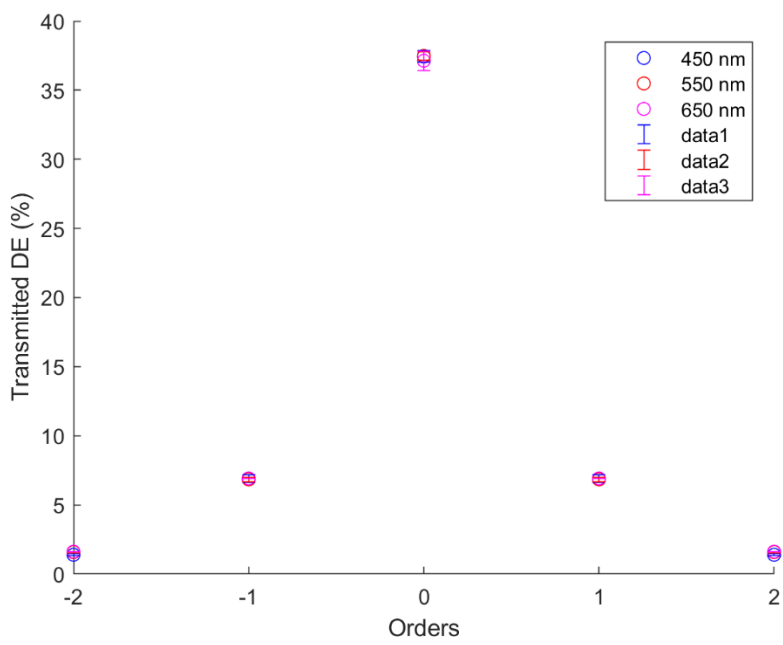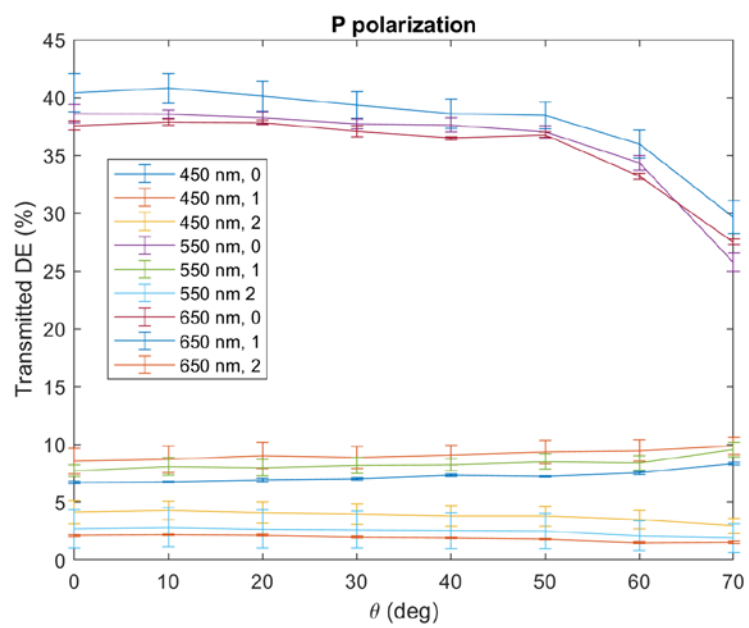
■ 1D square grating

□ Optical system setup

I changed the duty cycle to 36% to match your simulation. I also changed to system defini-
tion so that it could be tilted so that I could use the same k value each time.

```
(*Initial values of system*)
λInc = 550*^-3;

nMaterial = RefractiveIndex["Metal", "Cr", λInc][[2]];
gratingPeriod = 6.6; (*in microns*)
thickness = {0.08};
width = {{0, .64, 1}};(*36% duty cycle*)
index = {Flatten[{1., nMaterial}]};


(*width = {{0,0.25,0.75,1}};*)
(*index = {Flatten[{1.,nMaterial,1.}]};*)

(*Initial values for RCWA model*)
computedOrders = 20; (*number of Fourier terms used in algorithm*)
returnedOrders = {-2, -1, 0, 1, 2};

(*Defining optical system*)
```

```
opticalSystem[θ_] := {
   (*Diffraction Grating*)
   CreateSurface[ sys`surfID → 1,
     (*Define surface geometry*)
     sys`v → {0, 0, 0},
     sys`shape`type → "Plane",
     sys`aperture → Function[{x, y}, Abs[x] < 10 && Abs[y] < 10],
     sys`a → RotationMatrix[θ, {1, 0, 0}].{0, 0, 1},
     sys`material1 → "Air",
     sys`material2 → "Const_1.5",
     sys`mode → {"Refract", "Reflect"},

     (*Define the grating*)
     sys`coating`type → "RCWA",
     sys`coating`RCWA`ordersCalculate → computedOrders,
     sys`coating`RCWA`ordersReturned → returnedOrders,
     sys`coating`RCWA`gratingPeriod → gratingPeriod,
     sys`coating`RCWA`thicknessVec → thickness,
     sys`coating`RCWA`widthMatrix → width,
     sys`coating`RCWA`indexMatrix → index,
     sys`coating`RCWA`xLocal → RotationMatrix[θ, {1, 0, 0}].Normalize[{0, 1, 0}],
     (*direction of grating reptition*)
     sys`surfaceLabel → "Grating"],

   (*Collection surface*)
   CreateSurface[ sys`surfID → 2,
     sys`v → {0, 0, .05},
     sys`a → RotationMatrix[θ, {1, 0, 0}].{0, 0, 1},
     sys`shape`type → "Plane",
     sys`aperture → Function[{x, y}, Abs[x] < 1 && Abs[y] < 10],
     sys`material1 → "Const_1.5",
     sys`material2 → "Air",
     sys`mode → {"Refract"},
     sys`surfaceLabel → "Back surface" ],

   (*Collection surface*)
   CreateSurface[ sys`surfID → 3,
     sys`v → {0, 0, 20},
     sys`shape`type → "Plane",
     sys`aperture → Function[{x, y}, Abs[x] < 15 && -15 < y < 10],
     sys`material1 → "Air",
     sys`material2 → "Air",
     sys`mode → {"Refract"},
     sys`surfaceLabel → "Back surface" ]
   };
```

◻ Example ray trace

Trace rays over the angle range you plotted. I calculated the s transmission by multiplying
the cumulative Mueller matrices by {1,1,0,0} and taking the first component and I calcu-

lated p transmission by multiplying by {1,-1,0,0} and taking the first component. The curves shapes are very similar to your measurements but the values are a bit different, this is explained below.

```
endRaysTot = {};
testTot = {};
ordersOutTot = {};
Table[
  test = TraceRays[
    {CreateRay[ray`k → {0, 0, 1}, ray`λ → λInc, ray`r → {0, 0, -1}]}, opticalSystem[θ]];
  testTot = Append[testTot, test];
  endRays = Select[test, #[[ray`surfaceID]] == 3 && #[[ray`status]] == 1 &];
  endRays = endRays[[Ordering[ToExpression[StringSplit[#, " "][[-1]]] & /@
      endRays[[All, ray`modeLabel]]][[All, 2]]]]];
  ordersOutTot = Append[ordersOutTot, Sort[ToExpression[StringSplit[#, " "][[-1]]] & /@
      endRays[[All, ray`modeLabel]]][[All, 2]]]];
  endRaysTot = Append[endRaysTot, endRays];, {θ, 0, 70 / 180. * Pi, 70 / 180. * Pi / 10}];

θList = Table[θ, {θ, 0, 70 / 180. * Pi, 70 / 180. * Pi / 10}];
sTrans = Map[(#[[ray`MMCumulative]].{1, 1, 0, 0})[[1]] &, endRaysTot, {2}];
sTransSorted = Table[Transpose[{θList[[Position[ordersOutTot, order][[All, 1]]]],
      Extract[sTrans, Position[ordersOutTot, order]]}], {order, -2, 2}];
pTrans = Map[(#[[ray`MMCumulative]].{1, -1, 0, 0})[[1]] &, endRaysTot, {2}];
pTransSorted = Table[Transpose[{θList[[Position[ordersOutTot, order][[All, 1]]]],
      Extract[pTrans, Position[ordersOutTot, order]]}], {order, -2, 2}];
```

```
ListLinePlot[sTransSorted, PlotLegends → {"-2", "-1", "0", "1", "2"},
 PlotLabel → Style["s-polarized transmission", 16],
 PlotRange → {All, {0, .45}}, AxesLabel → {"Wavelength μm", "Trans"}]
ListLinePlot[pTransSorted, PlotLegends → {"-2", "-1", "0", "1", "2"},
 PlotLabel → Style["p-polarized transmission", 16],
 PlotRange → {All, {0, .45}}, AxesLabel → {"Wavelength μm", "Trans"}]
```

s–polarized transmission


p–polarized transmission
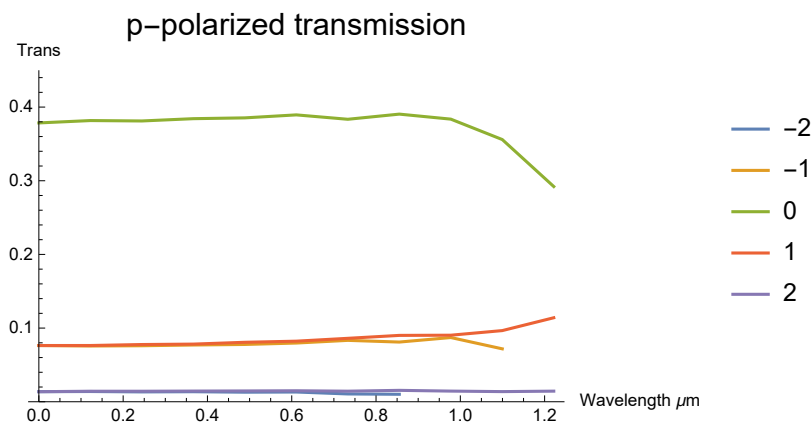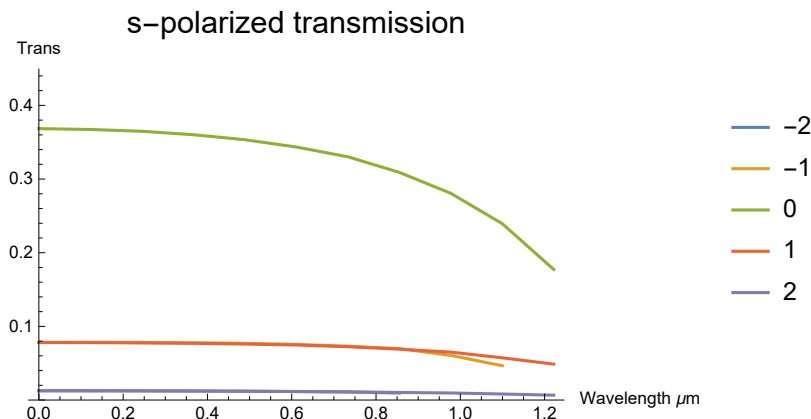
Your presentation says that for your experiment methodology you multiply the value by 0.96 to account for Fresnel losses. If I multiply my results by 0.96 they would be more different from your experimental results. Multiplying by 0.96 also doesn't account for Fresnel losses, it would basically be adding an extra surface worth of Fresnel losses. I am guessing you actually, correctly divided by 0.96 and if I do that the simulation matches your experimental results quite well.

```
θList = Table[θ, {θ, 0, 70 / 180. * Pi, 70 / 180. * Pi / 10}];
sTrans = Map[(#[[ray`MMCumulative]].{1, 1, 0, 0})[[1]] &, endRaysTot, {2}];
sTransSorted = Table[Transpose[{θList[[Position[ordersOutTot, order][[All, 1]]]],
     1 / .96 * Extract[sTrans, Position[ordersOutTot, order]]}], {order, -2, 2}];
pTrans = Map[(#[[ray`MMCumulative]].{1, -1, 0, 0})[[1]] &, endRaysTot, {2}];
pTransSorted = Table[Transpose[{θList[[Position[ordersOutTot, order][[All, 1]]]],
     1 / .96 * Extract[pTrans, Position[ordersOutTot, order]]}], {order, -2, 2}];
```
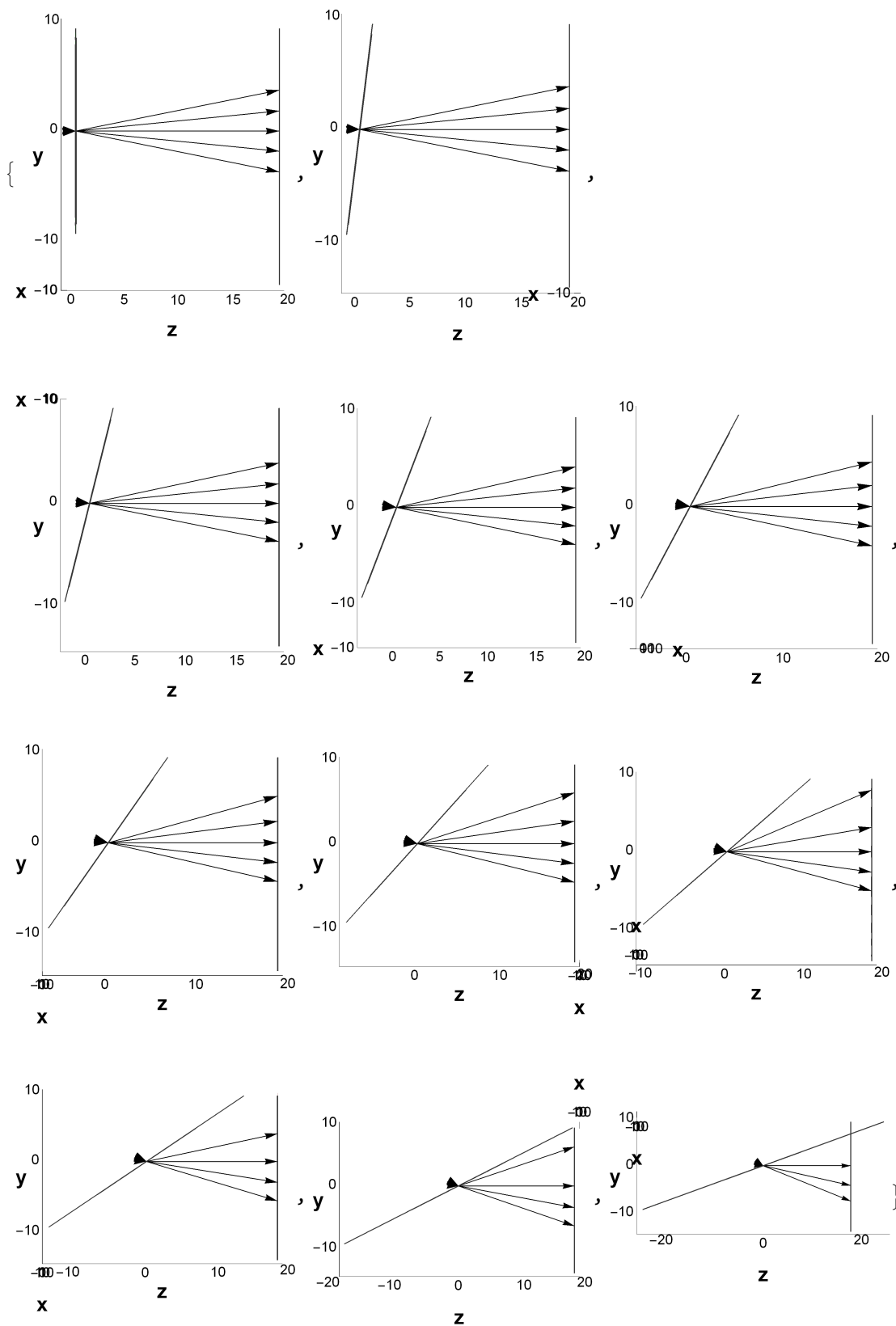
```
ListLinePlot[sTransSorted, PlotLegends → {"-2", "-1", "0", "1", "2"},
 PlotLabel → Style["s-polarized transmission", 16],
 AxesLabel → {"Wavelength μm", "Trans"}]
ListLinePlot[pTransSorted, PlotLegends → {"-2", "-1", "0", "1", "2"},
 PlotLabel → Style["p-polarized transmission", 16], AxesLabel → {"Wavelength μm", "Trans"}]
```
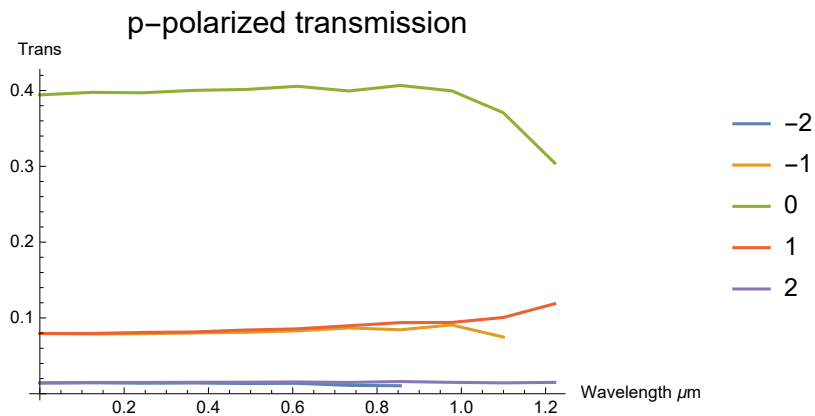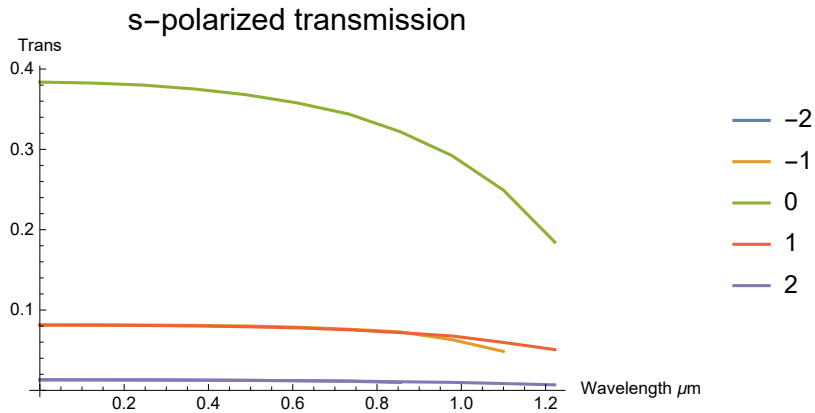
`MapThread[PlotSystem[#1, opticalSystem[#2]] &, {testTot, θList}]`

References

[1] A. Sommerfeld. *Optics,* Volume IV of *Lectures on Theoretical Physics*. Academic Press, Inc., New York, 1954.

[2] J. W. Goodman. *Introduction to Fourier Optics*. Roberts & Company, Greenwood Village, Colorado. 2005.

[3] M. C. Hutley. "An experimental study of anomalies of sinusoidal diffraction gratings." *Optica Acta: International Journal of Optics* 20. 607-624. 1973.

[4] J. Harvey and R. Pfisterer. "Parametric diffraction efficiency of non-paraxial sinusoidal reflection gratings." Tucson, Arizona. 2017.

[5] The Theory of Gratings (2013), In T. D. Milster (Comp.), OPTI 505R: Diffraction and Interferometry, Chapter 5.5, Tucson, Arizona: The University of Arizona.

[6] R. Petit. *Topics in Current Physics, Electromagnetic Theory of Gratings*. Springer-Verlag Berlin Heidelberg. 1980.

[7] H. Kogelnik. "Coupled wave theory for thick hologram gratings." *The Bell System Technical Journal* 48. 2909-2947. 1969.

[8] R. Chu and J. Kon. "Modal theory for spatially periodic media." *IEEE Transactions on Microwave Theory and Techniques* MTT-25. 18-24. 1977.

[9] M. G. Moharam and T.K. Gaylord. "Rigorous coupled-wave analysis of planar-grating diffraction." *J. Opt. Soc. Am.* 71. 811-818. 1981.

[10] M.G. Moharam and T. K. Gaylord. "Diffraction analysis of dielectric surface-relief gratings." *J. Opt. Soc. Am.* 72. 1385-1392. 1982.

[11] R. C. Rumpf. "Improved Formulation of Scattering Matrices for Semi-Analytical Methods that is Consistent with Convention." *Progress In Electromagnetics Research B* 35. 241-261. 2011.

[12] A. Hessel and A. A. Oliner. "A New Theory of Wood's Anomalies on Optical Gratings." *Applied Optics* 4. 1275-1297. 1965.

[13] J. Harvey, et al. "Diffracted radiance: a fundamental quantity in nonparaxial scalar diffraction theory." *Applied Optics* 38. 6469-6481. 1999.

[14] J. E. Harvey and R. N. Pfisterer. "Understanding Diffraction Grating Behavior: Part I: Including Conical Diffraction & Rayleigh Anomalies from Transmission Gratings." Tucson, Arizona. Unpublished manuscript.

 [15] P. Lalanne and E. Silberstein. "Fourier-modal methods applied to waveguide computational problems." *Optics Letters* 25. 1092-1094. 2000.

[16] T. Zebrowski, et al. "Simulation of Liquid Crystal Infiltrated Photonic Crystal Fibers Using the Fourier Modal Method." *Optical Society of America*. 2010.

[17] A. Taghizadeh. "Numerical Investigation of Vertical Cavity Lasers with Subwavelength Gratings Using the Fourier Modal Method." *Journal of Lightwave Technology*. 2016.

[18] Airy Optics, Polaris M. Retrieved from https://www.airyoptics.com/Polaris-M_Description.pdf

[19] Synopsis, DiffractMOD. Retrieved from https://www.synopsys.com/optical-solutions/rsoft/passive-device-diffractMOD.html

[20] Stanford University, S4. Retrieved from https://web.stanford.edu/group/fan/S4/

[21] Formulation of Rigorous Coupled-Wave Analysis (2013), In R. Rumpf, EE 5337: Computational Electromagnetics, Lecture 19, El Paso, Texas: The University of Texas.

[22] E. Hecht. *Optics*. Addison-Wesley. 2002.

[23] Multilayer Films, In J. C. Wyant (Comp.), OPTI 505R: Diffraction and Interferometry, Chapter 8, Tucson, Arizona: The University of Arizona.

[24] Fraunhofer diffraction from thin gratings (2013), In T. D. Milster (Comp.), OPTI 505R: Diffraction and Interferometry, Chapter 5.5.2, Tucson, Arizona: The University of Arizona.

[25] Conversation with Edmund Optics